Adaptive dynamic fracture simulation using potential-based cohesive zone modeling and polygonal finite elements

Sofie Leon

University of Illinois
Department of Civil and Environmental Engineering

July 31st, 2013

Seminar at Sandia National Laboratory
Livermore, California

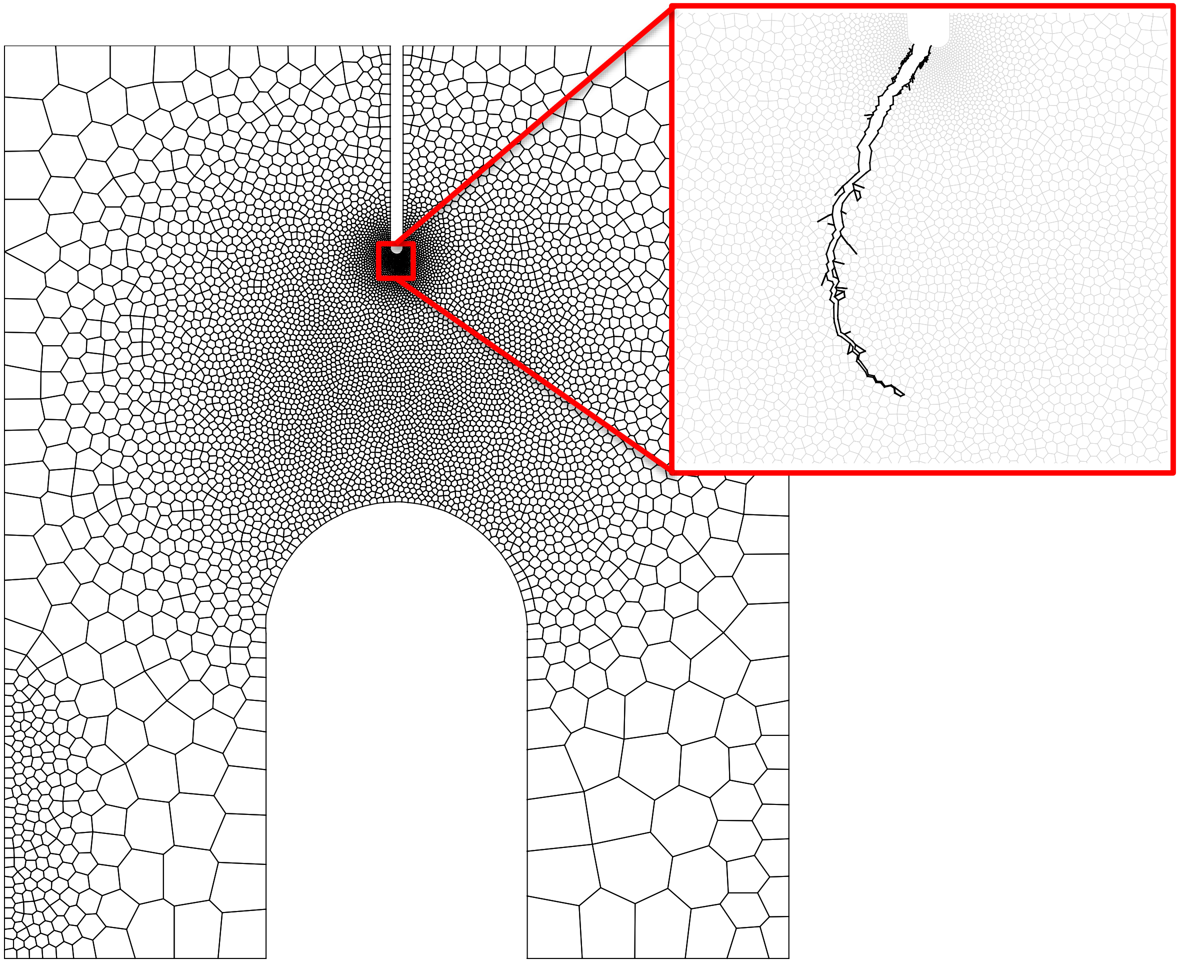

Sandia National Laboratories

About me…

- Graduate student in Civil Engineering at the University of Illinois at Urbana-Champaign

- Undergrad at Cal Poly, San Luis Obispo, CA

- Originally from Ventura, CA

Acknowledgements

Daniel Spring

Professor Glaucio H. Paulino,
Research Advisor

National Science Foundation
Graduate Research Fellowship Program

Outline: Tools for dynamic fracture simulation on polygonal discretizations

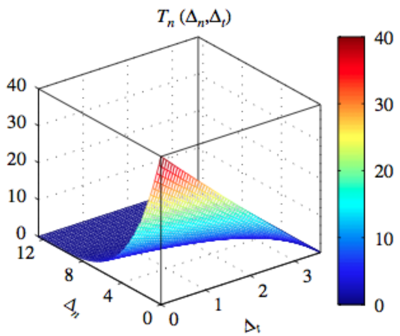

Dynamic fracture with interfacial cohesive zone modeling

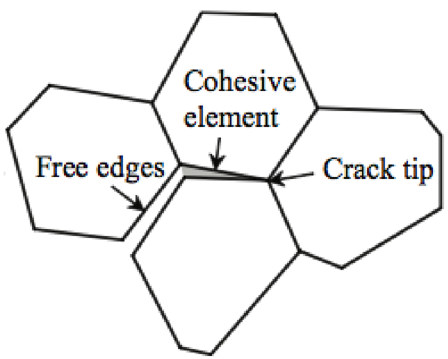

Dynamic fracture simulation with CVT polygonal finite elements

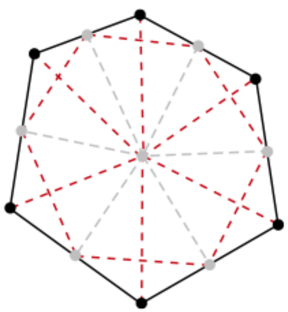

Adaptive topological operators for polygonal finite elements

Outline: Tools for dynamic fracture simulation on polygonal discretizations

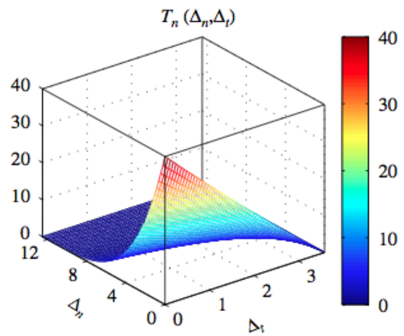

Dynamic fracture with interfacial cohesive zone modeling

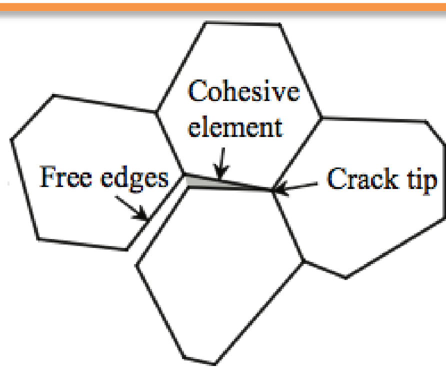

Dynamic fracture simulation with CVT polygonal finite elements

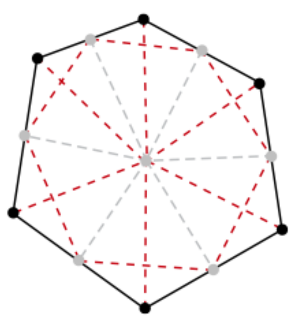

Adaptive topological operators for polygonal finite elements

Cohesive elements aim to capture the highly nonlinear behavior in the zone ahead of a crack tip

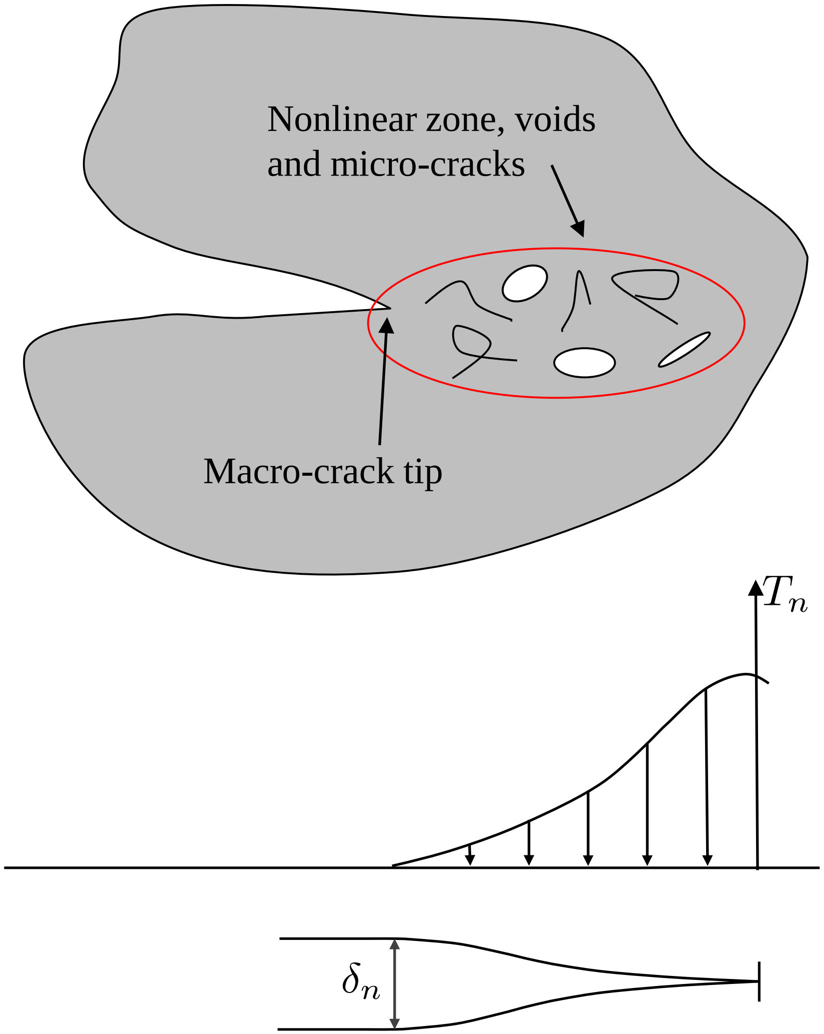

When the size of the nonlinear zone ahead of a crack tip is not negligible, for example in ductile or quasi-brittle materials, the LEFM may not be appropriate

In the inter-element approach, cohesive elements are inserted at the facets of bulk elements

Cohesive elements consist of two facets that can separate from each other by means of a traction separation relation

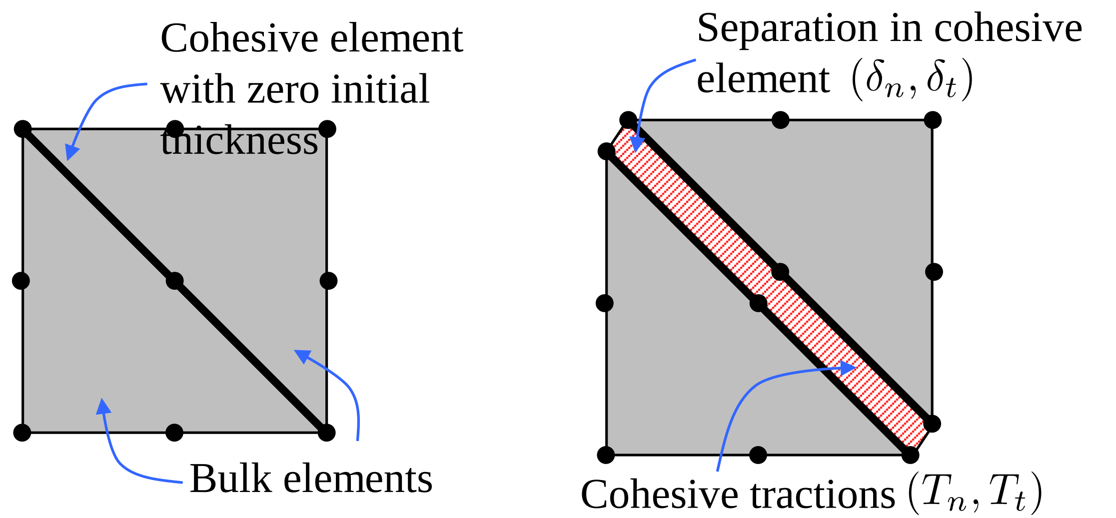

FEM analysis → displacements → cohesive constitutive relation → tractions

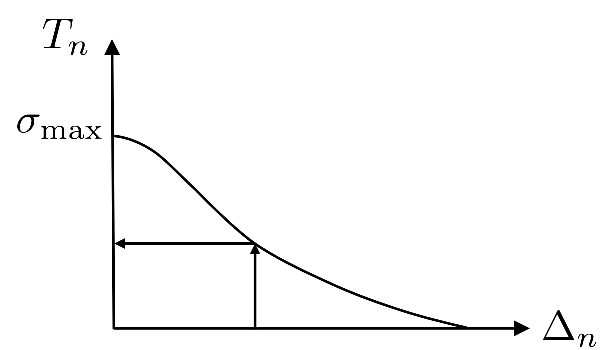

In the inter-element approach, cohesive elements are inserted at the facets of bulk elements

Cohesive elements consist of two facets that can separate from each other by means of a traction separation relation

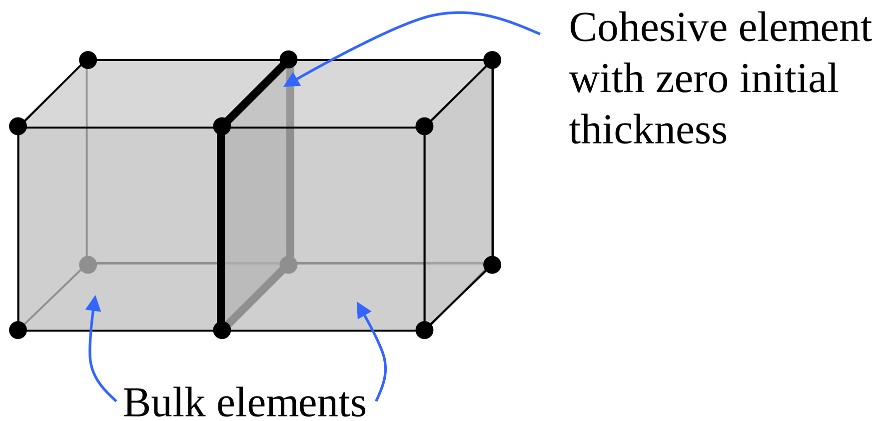

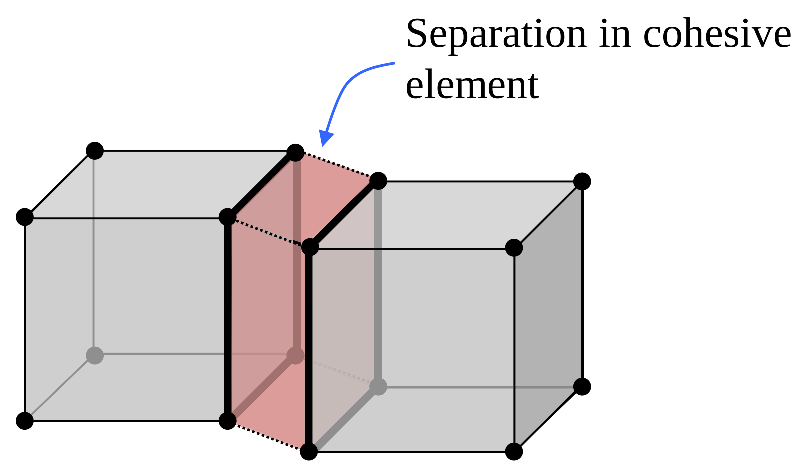

FEM analysis → displacements → cohesive constitutive relation → tractions

The PPR is an attractive model for cohesive failure simulation

The traction-separation relation is valid only in the area of influence

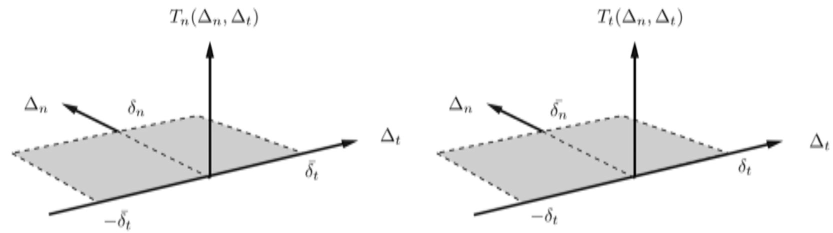

Critical boundary conditions are obeyed even when properties are different in each mode

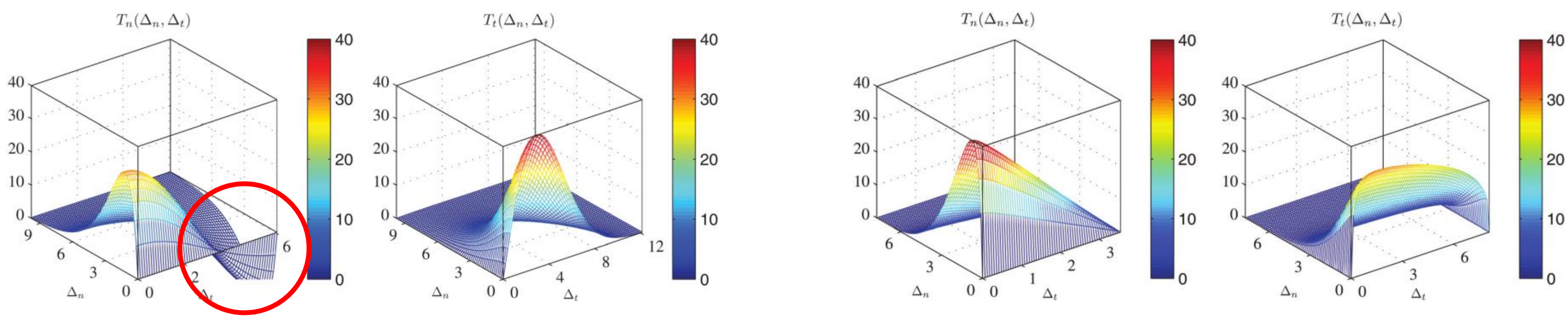

User had control over key material parameters

Fracture energies: ϕ_n, ϕ_t Cohesive strengths: σ, τ

Shape of softening: α, β Initial slope: λ_n, λ_t

Park, K., & Paulino, G. H. *AMR*, 64(6), 060802, 2013.
Xu, X. P., and Needleman, *A. Model. Simul. Mater. Sci. Eng.*, 1(2), pp. 111–13, 1993.

We employ the extrinsic approach in which a stress criteria is used to insert cohesive elements

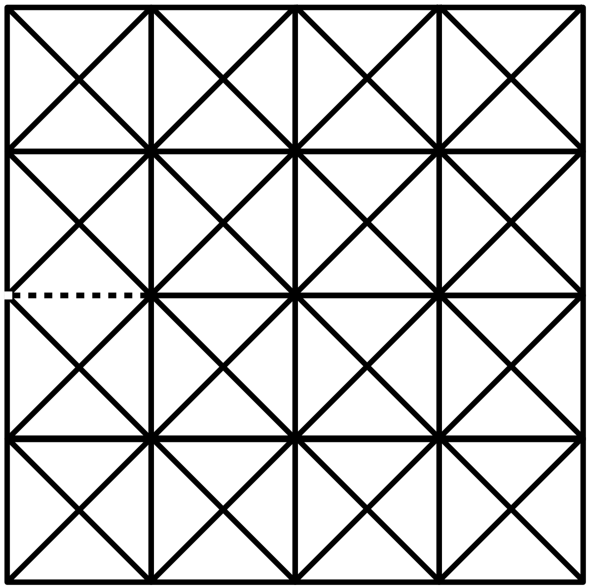

Consider a domain with an initial notch (dashed line)

Stresses are computed from displacements and extrapolated to the nodes

We employ the extrinsic approach in which a stress criteria is used to insert cohesive elements

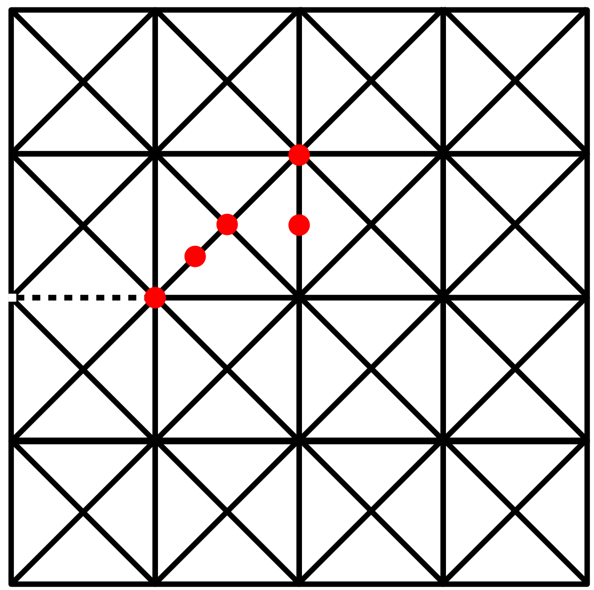

Consider a domain with an initial notch (dashed line)

Stresses are computed from displacements and extrapolated to the nodes

Nodes with stress greater than 90% of the cohesive strength of the material are flagged for further investigation

We employ the extrinsic approach in which a stress criteria is used to insert cohesive elements

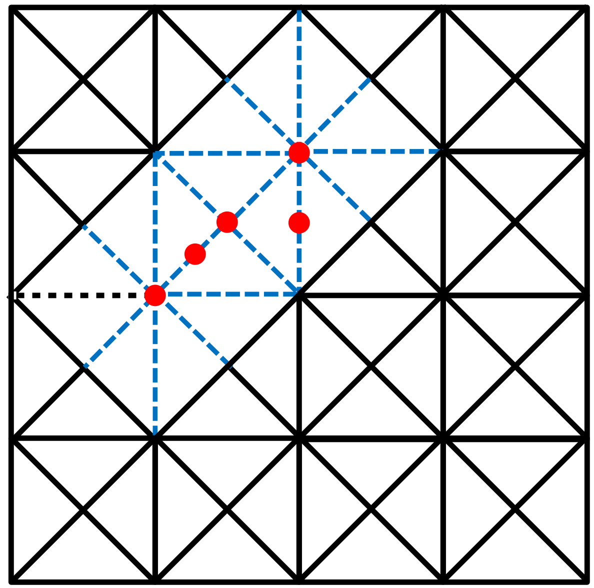

Compute the principle stress along the facets adjacent to the flagged nodes

If the stress is greater than the cohesive strength, insert a cohesive element

The dynamic simulation is carried out by means of an explicit time integration scheme

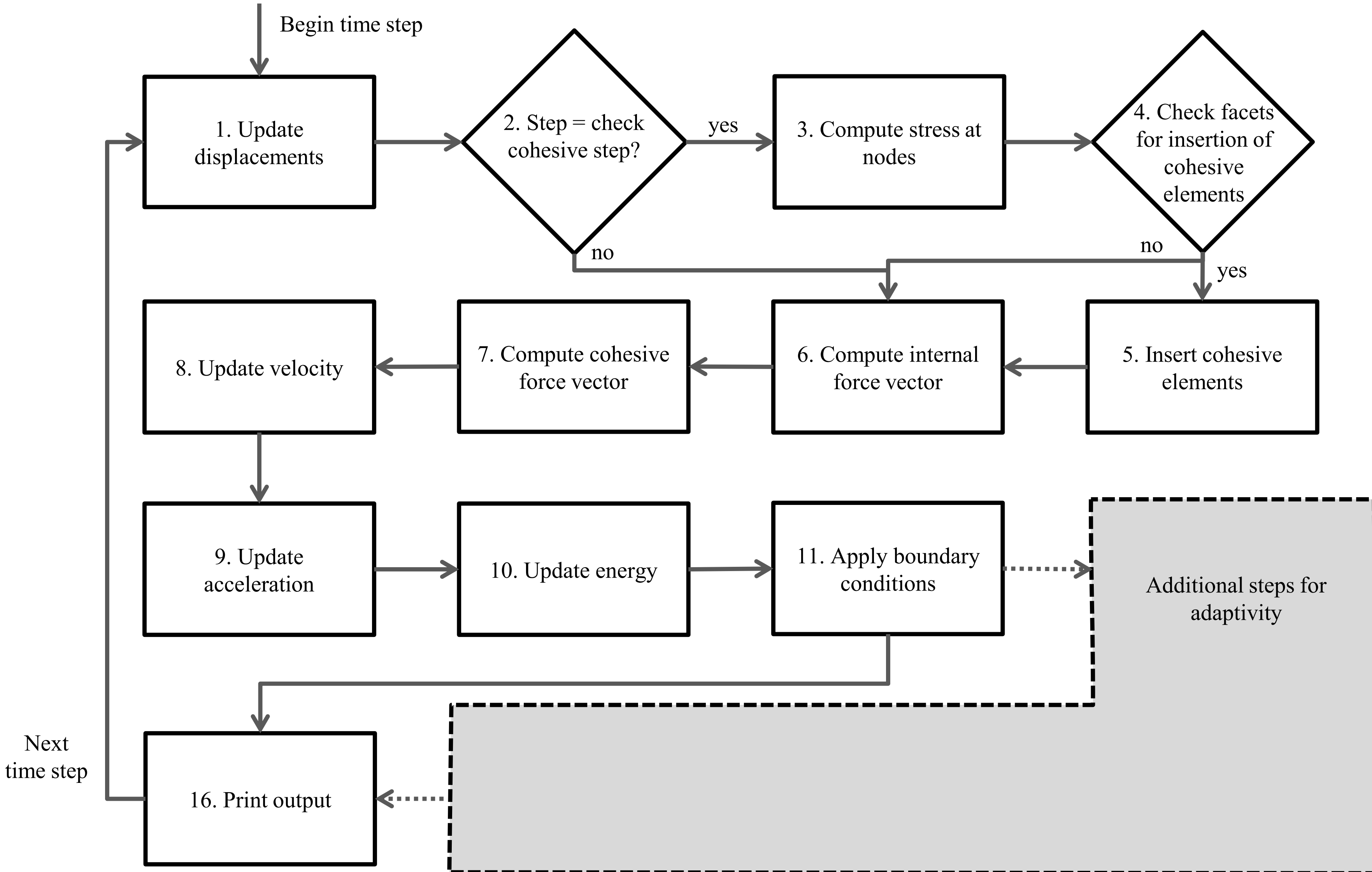

Outline: Tools for dynamic fracture simulation on polygonal discretizations

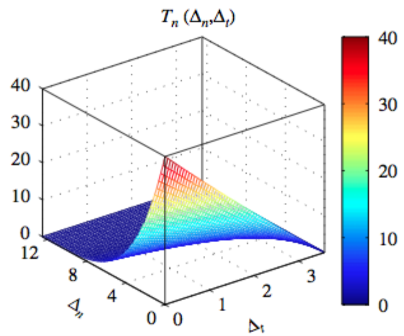

Dynamic fracture with interfacial cohesive zone modeling

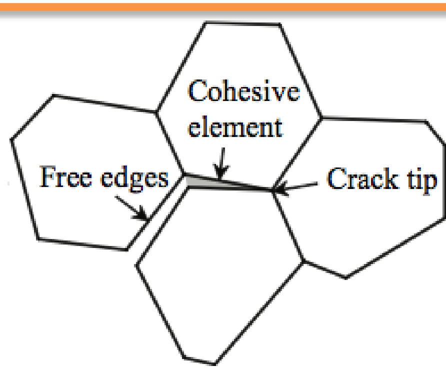

Dynamic fracture simulation with CVT polygonal finite elements

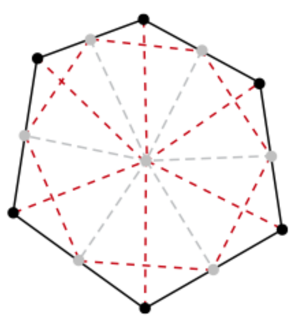

Adaptive topological operators for polygonal finite elements

Outline: Tools for dynamic fracture simulation on polygonal discretizations

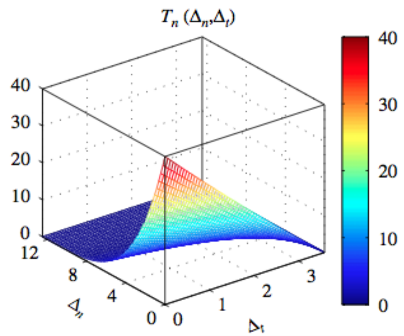

Dynamic fracture with interfacial cohesive zone modeling

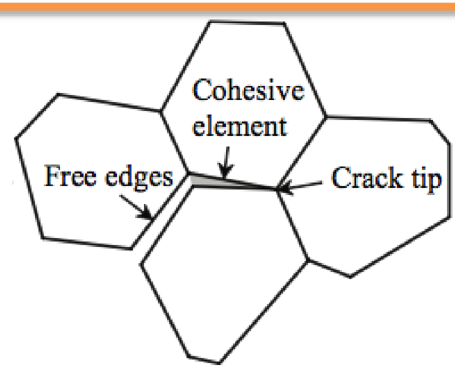

Dynamic fracture simulation with CVT polygonal finite elements

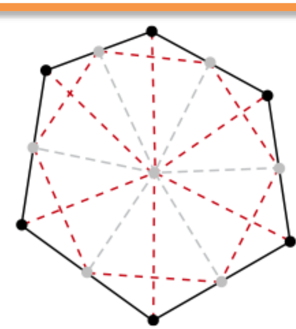

Adaptive topological operators for polygonal finite elements

Crack patterns on structured grids may be biased by the mesh

4k structured mesh is commonly used in fracture simulation

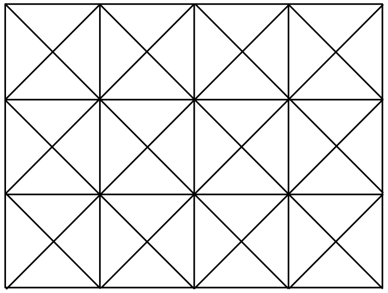

Crack patterns on the structured 4k mesh are limited by the element facets

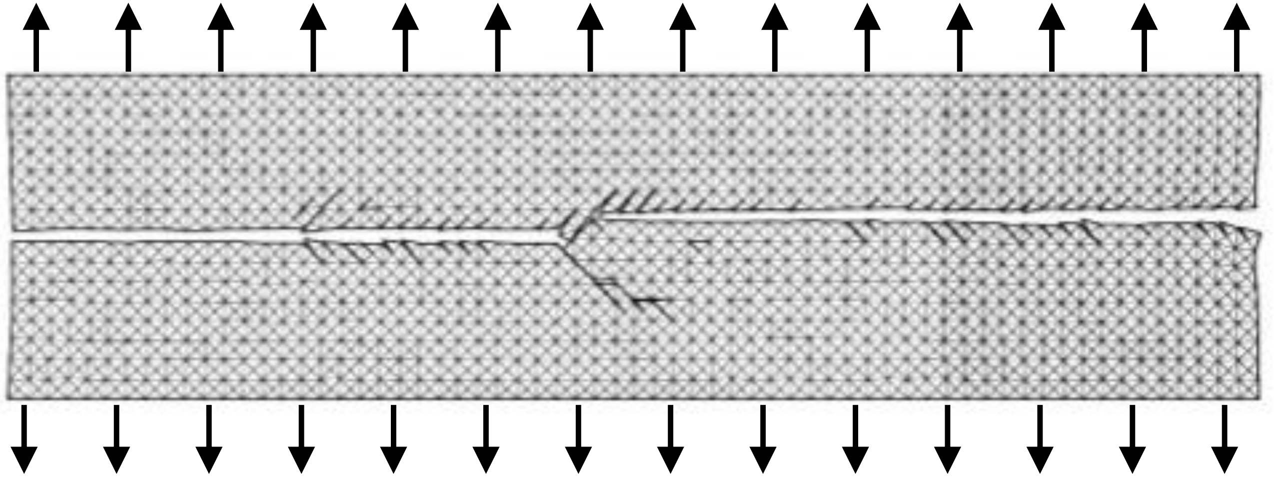

Zhang, Z., Paulino, G., & Celes, W. *IJNME*, 72(8), 893–923, 2007.

Mesh adaptivity operators are introduced improve fracture patterns

Original 4k mesh

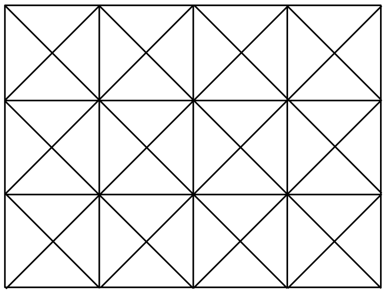

Nodal perturbation

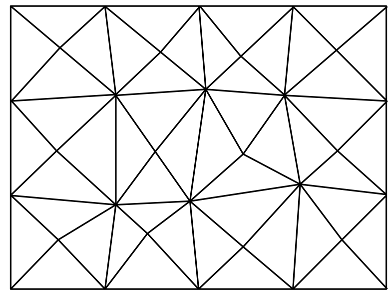

Original 4k mesh

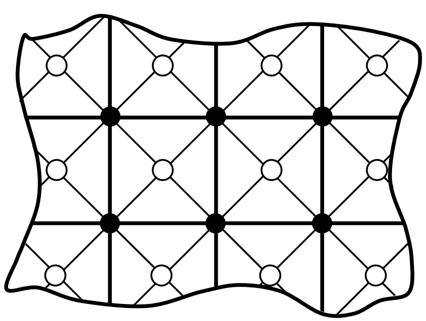

Edge swap

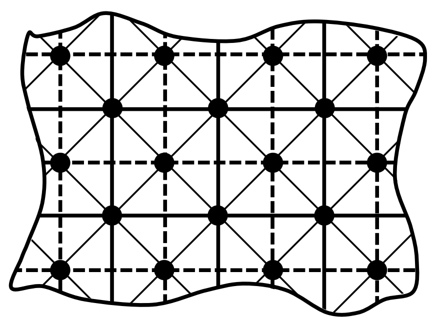

Mesh refinement

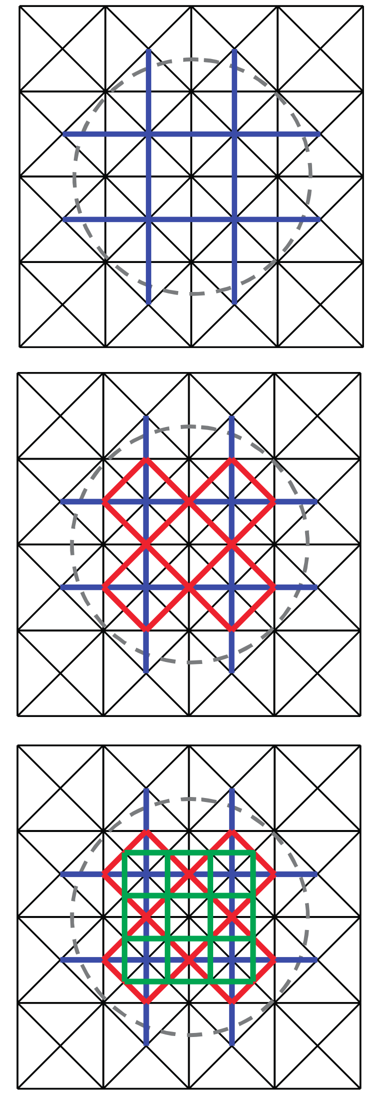

Paulino, G. H., Park, K., Celes, W., & Espinha, R. *IJNME*, 84(11), 1303–1343. 2010.
Park, K., Paulino, G. H., Celes, W., & Espinha, R. *IJNME*, 92(1), 1–35, 2012.

Even with adaptive operators, structured meshes exhibit bias for crack propagation

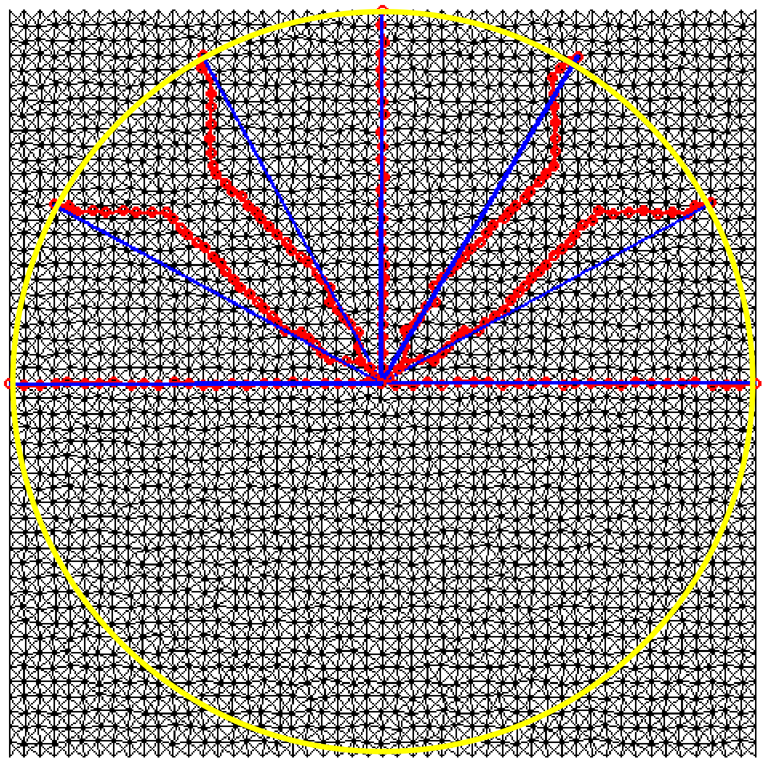

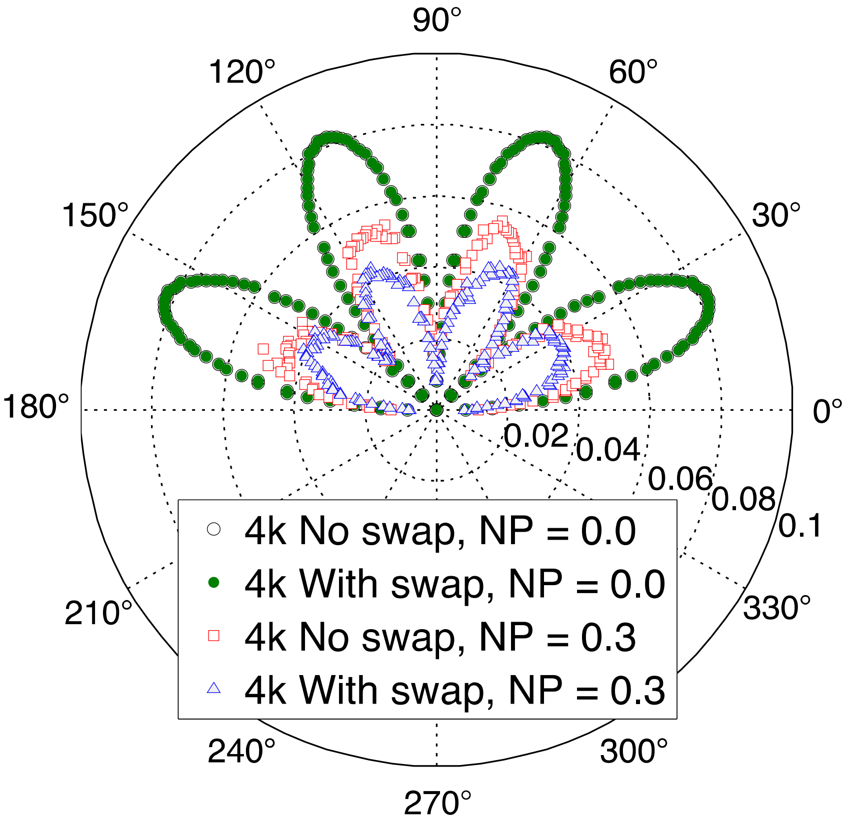

FEM distance measured with Dijkstra's algorithm

Error in crack length is dependent on angle of propagation

Rimoli, J. J. & Rojas, J. J., "Meshing strategies for the alleviation of mesh-induced effects in cohesive element models," submitted. Preprint: http://arxiv.org/abs/1302.1161

Instead of structured meshes, we use CVT polygonal discretizations

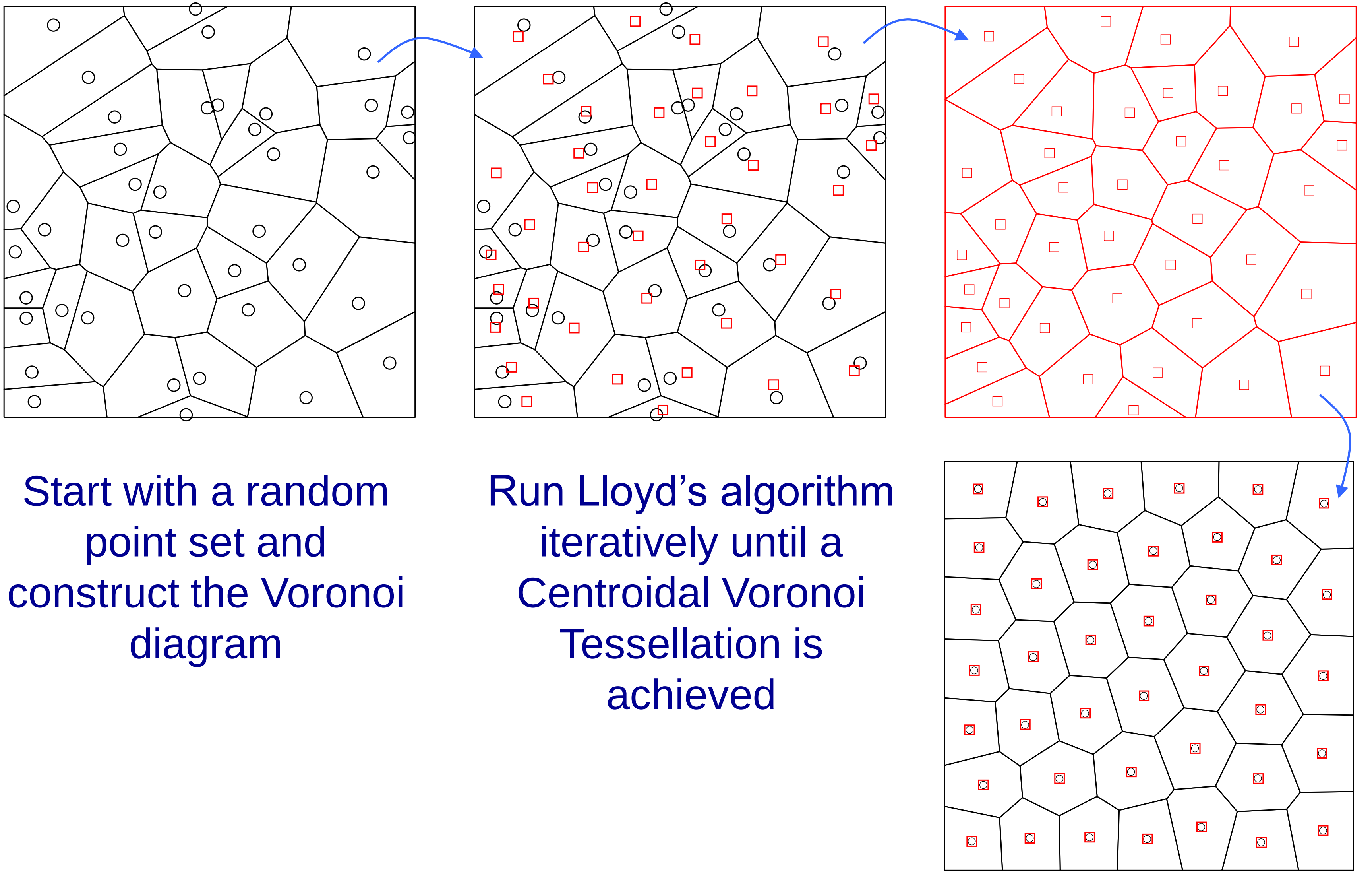

Start with a random point set and construct the Voronoi diagram

Run Lloyd's algorithm iteratively until a Centroidal Voronoi Tessellation is achieved

Talischi, C., Paulino, G. H., Pereira, A., & Menezes, I. F. M. *JSMO* 45(3), 309–328, 2012.

We can construct graded meshes using a non-constant density function in Lloyd's algorithm

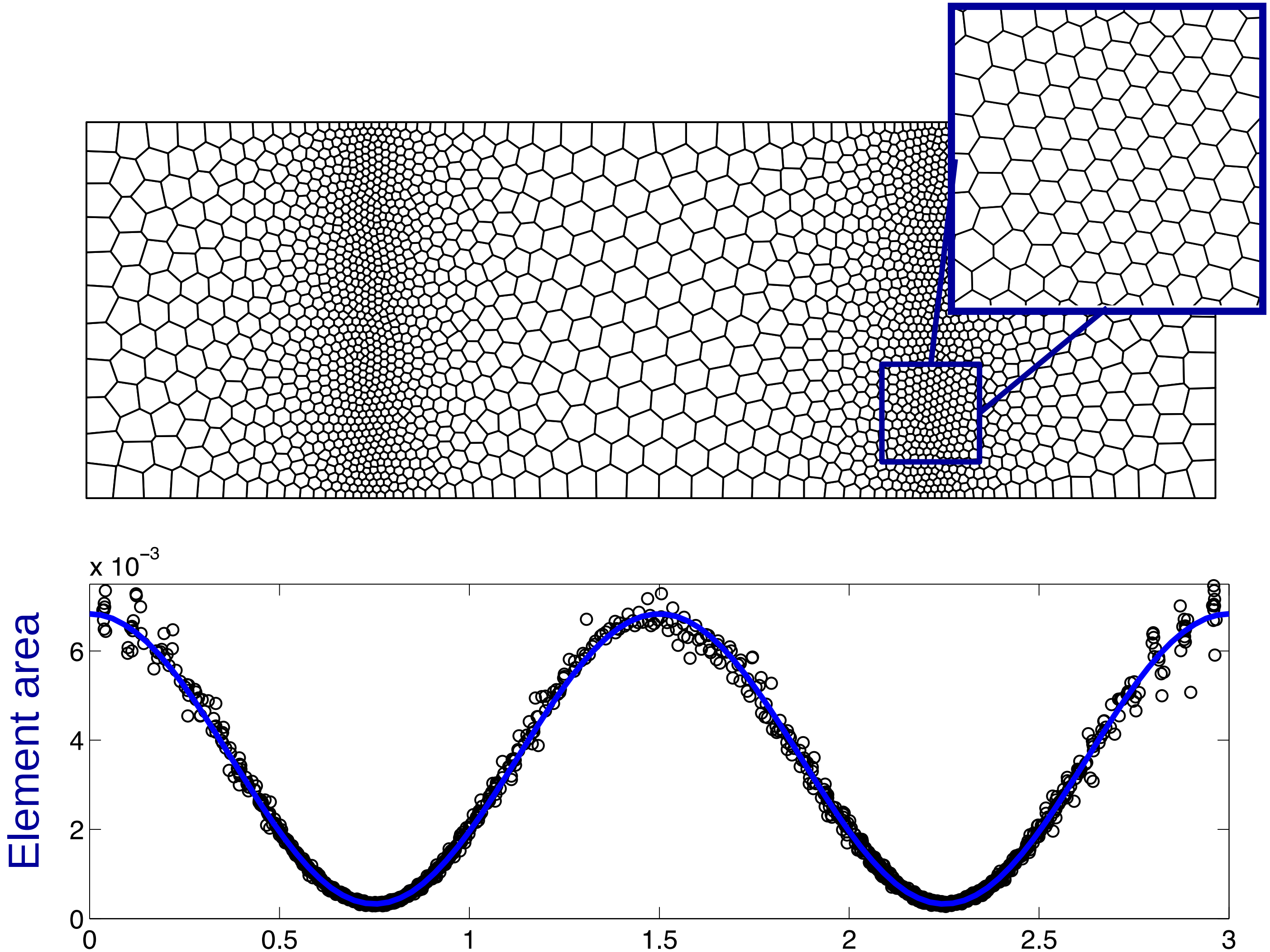

Talischi, C., Paulino, G. H., Pereira, A., & Menezes, I. F. M. *JSMO* 45(3), 309–328, 2012.

CVT meshes provide an alternative to structured meshes that reduces mesh bias

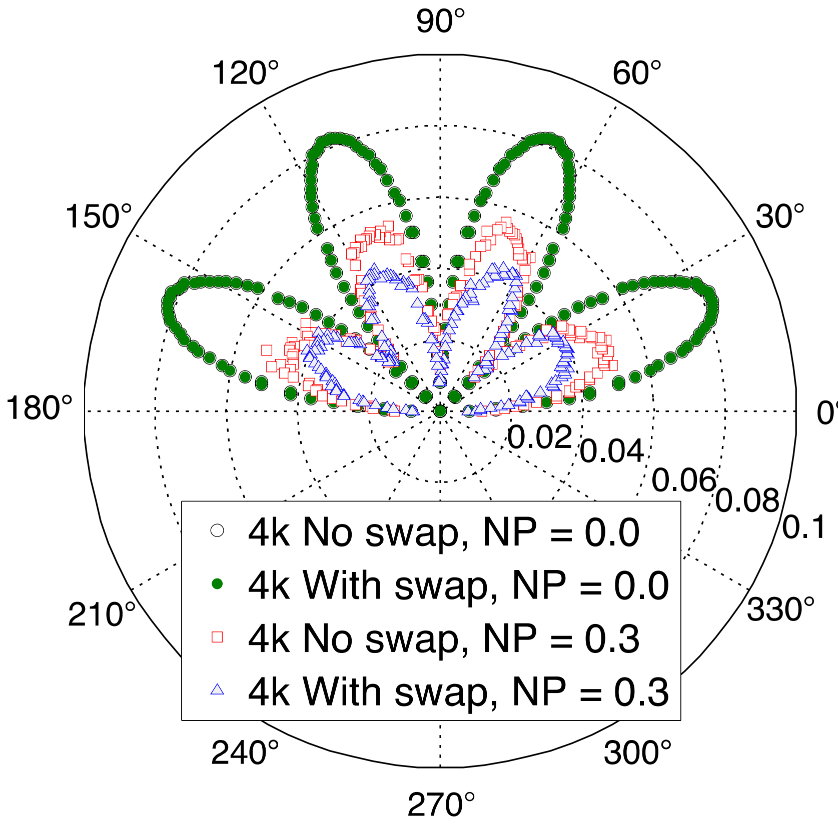

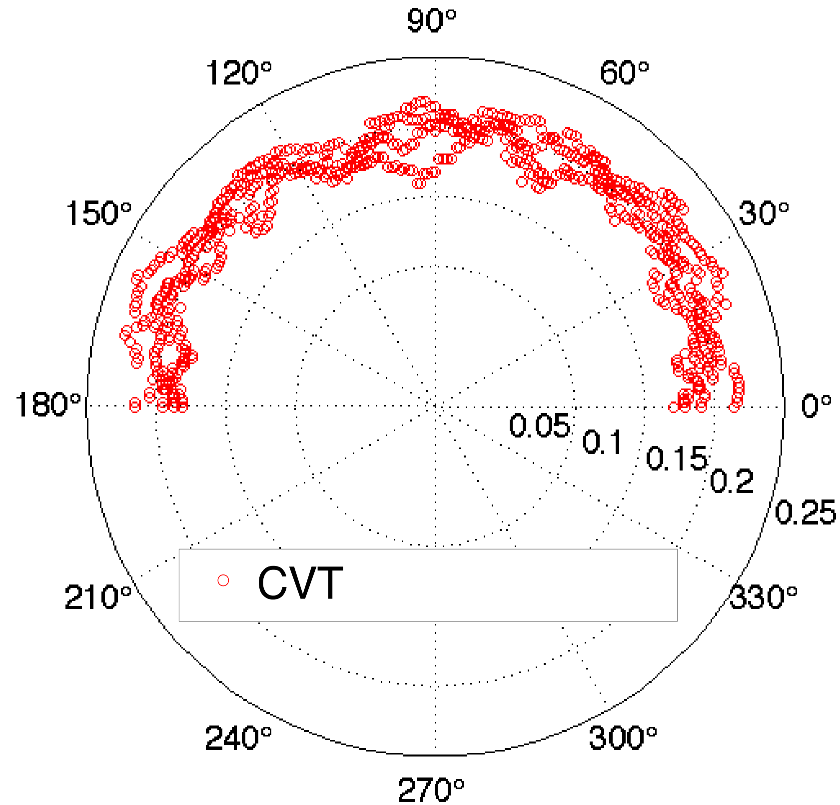

Crack length studies show the CVT meshes are isotropic

However, error is significantly higher than the 4k mesh

Leon, S. E., Spring, D. W., & Paulino, G. H. Submitted to *IJNME*.ç

Dynamic fracture simulations with polygonal elements led to unrealistic results

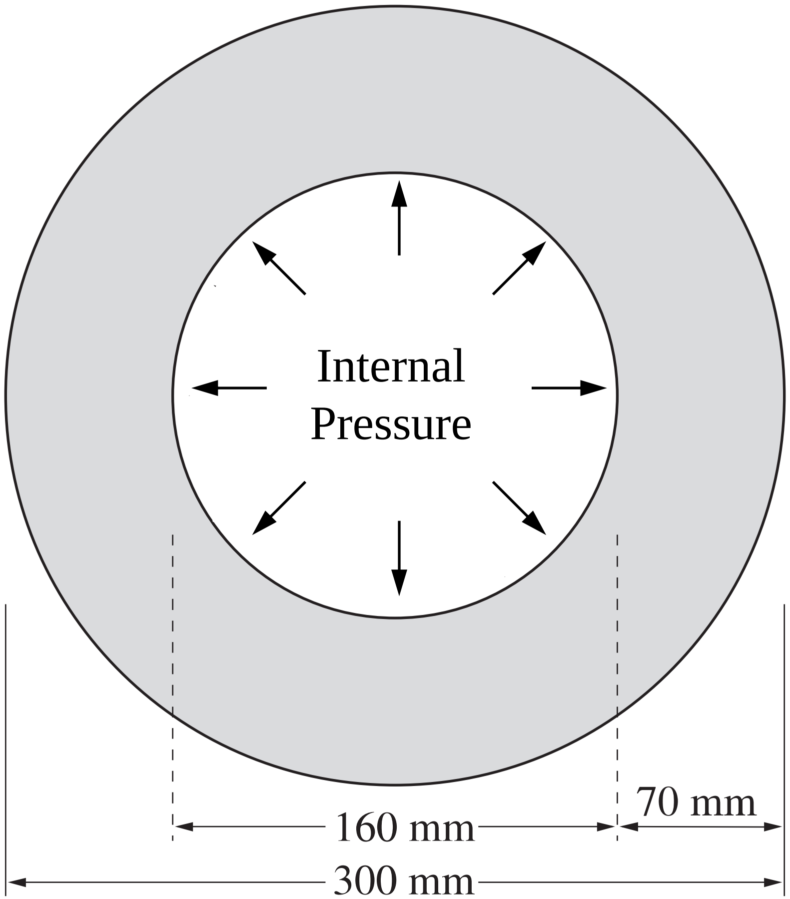

Expected result contains complete fragments

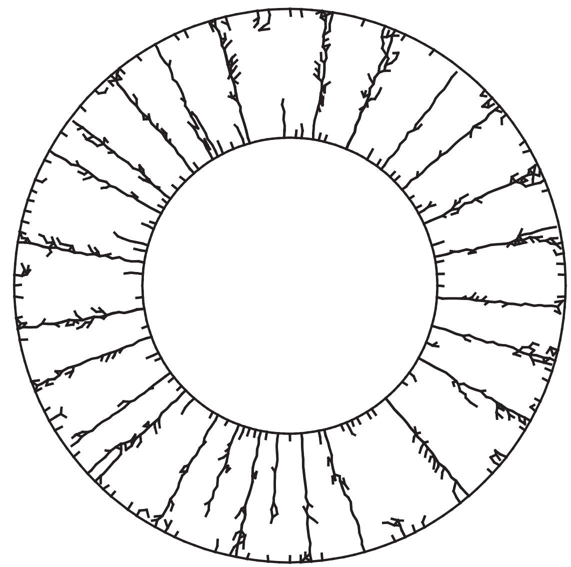

Paulino, G. H., Park, K., Celes, W., & Espinha, R. *IJNME*, 84(11), 1303–1343. 2010.

Dynamic fracture simulations with polygonal elements led to unrealistic results

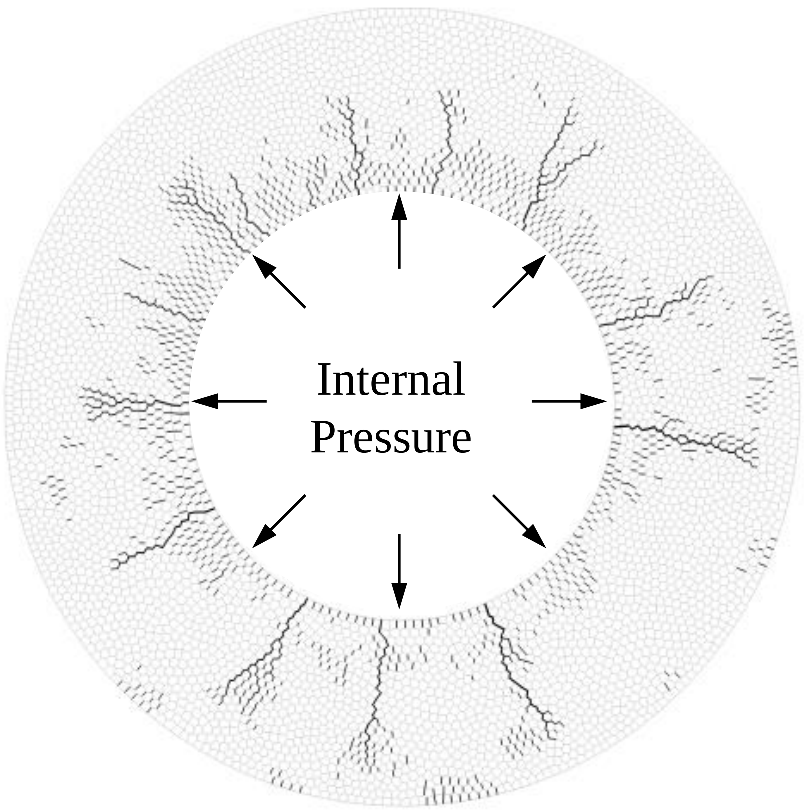

Expected result contains complete fragments

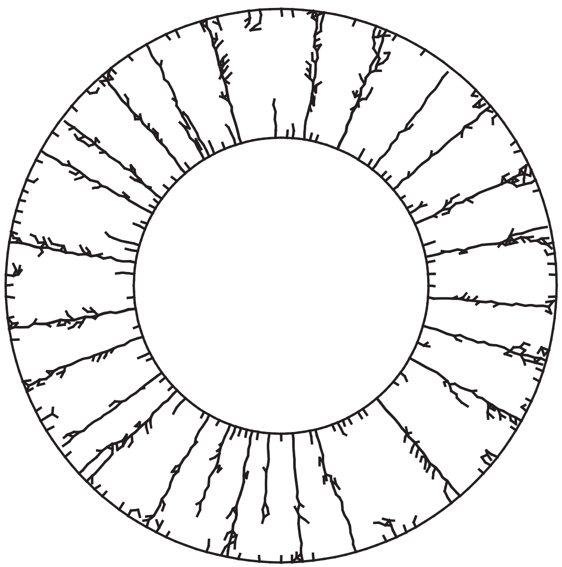

Even as the mesh is refined, the crack patterns do not converge to the expected result

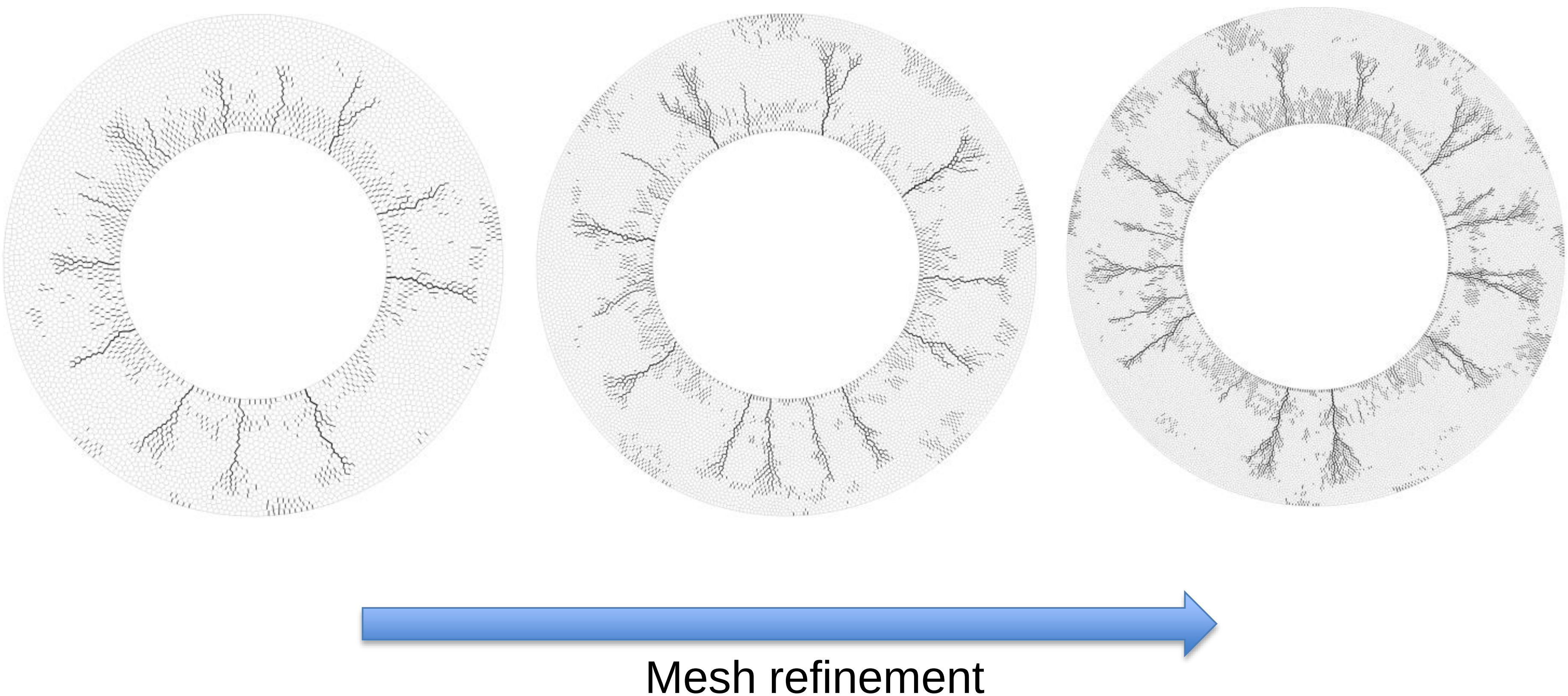

Poor results are explained by the lack of available crack directions in a CVT mesh

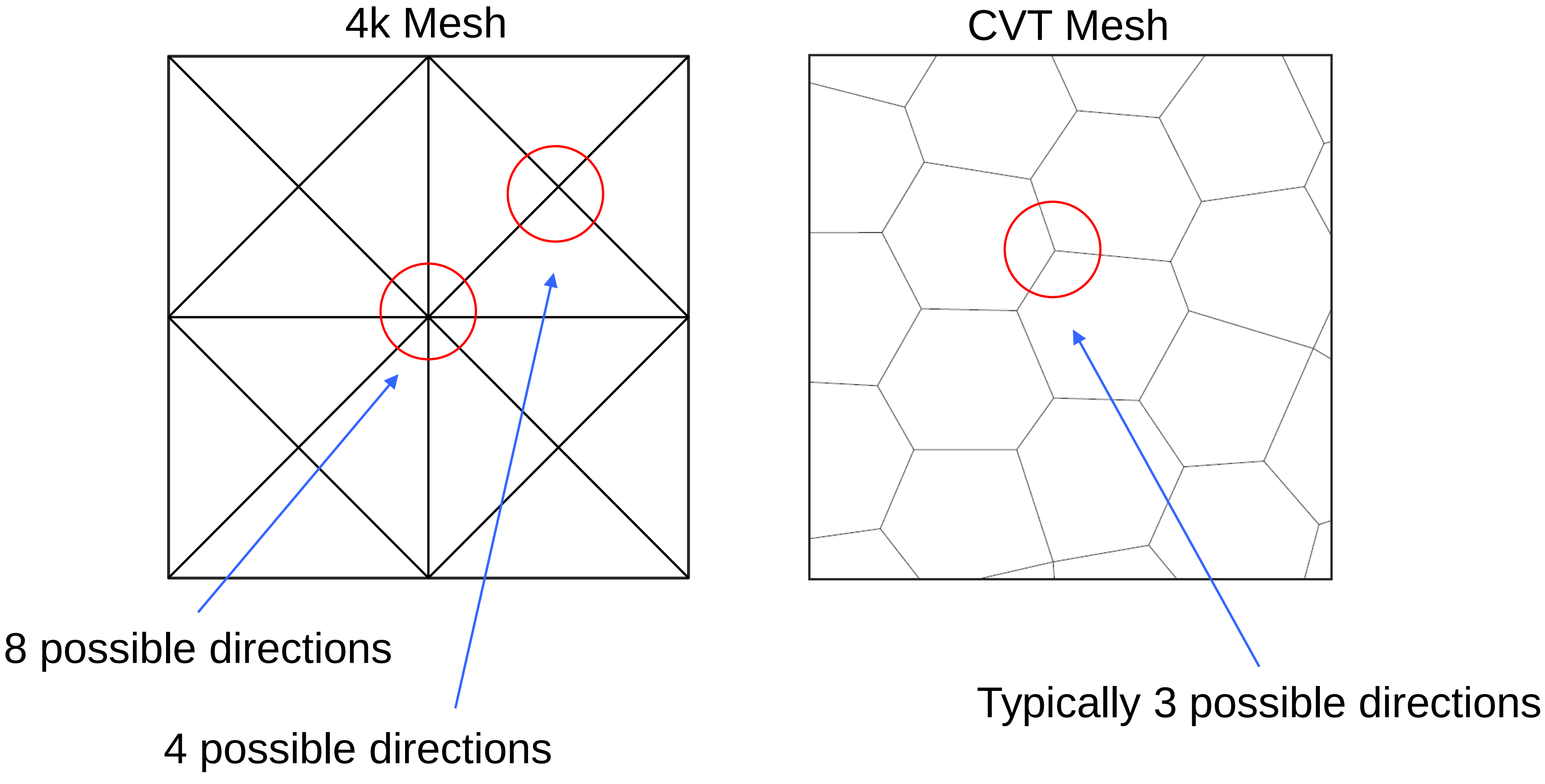

Outline: Tools for dynamic fracture simulation on polygonal discretizations

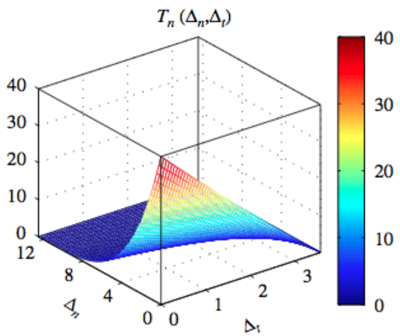

Dynamic fracture with interfacial cohesive zone modeling

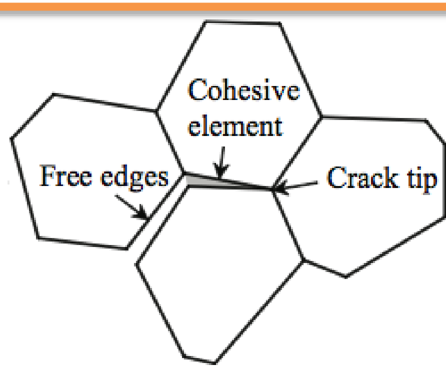

Dynamic fracture simulation with CVT polygonal finite elements

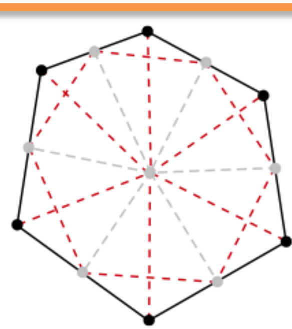

Adaptive topological operators for polygonal finite elements

Outline: Tools for dynamic fracture simulation on polygonal discretizations

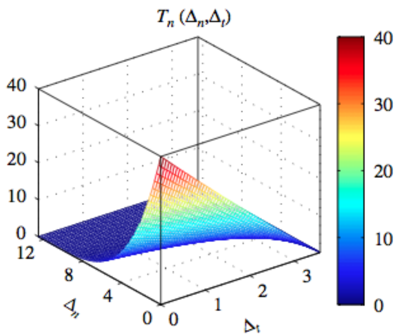

Dynamic fracture with interfacial cohesive zone modeling

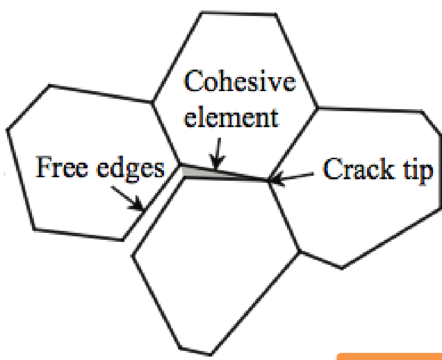

Dynamic fracture simulation with CVT polygonal finite elements

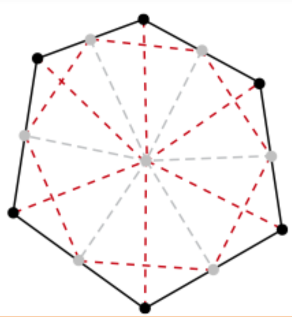

Adaptive topological operators for polygonal finite elements

We introduce element splitting to provide more directions for the crack to propagate

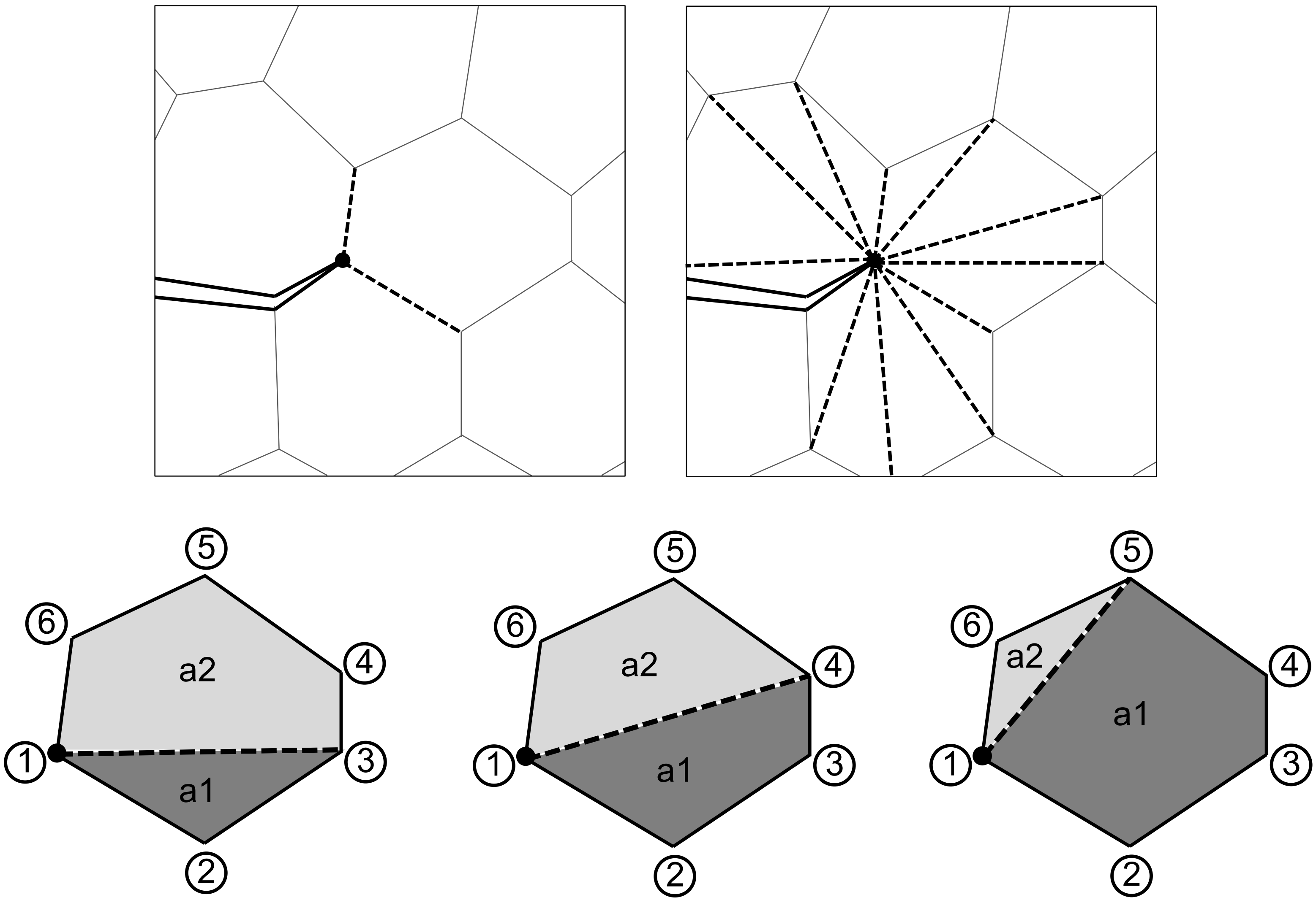

To avoid poorly shaped elements, we limit the available nodes for element splitting

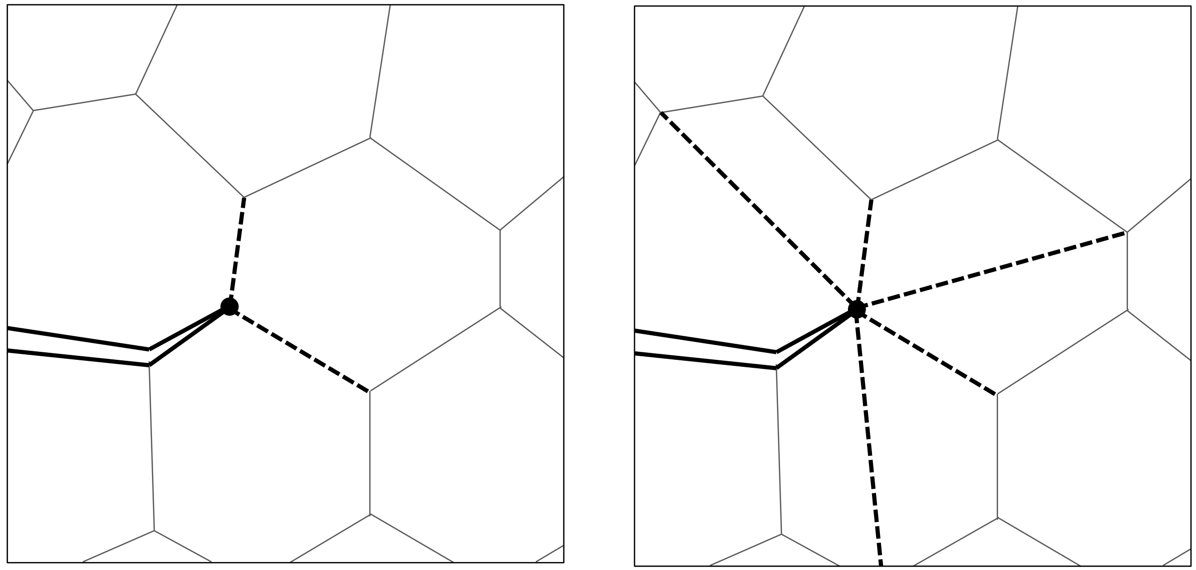

Choose the node that minimizes difference in areas

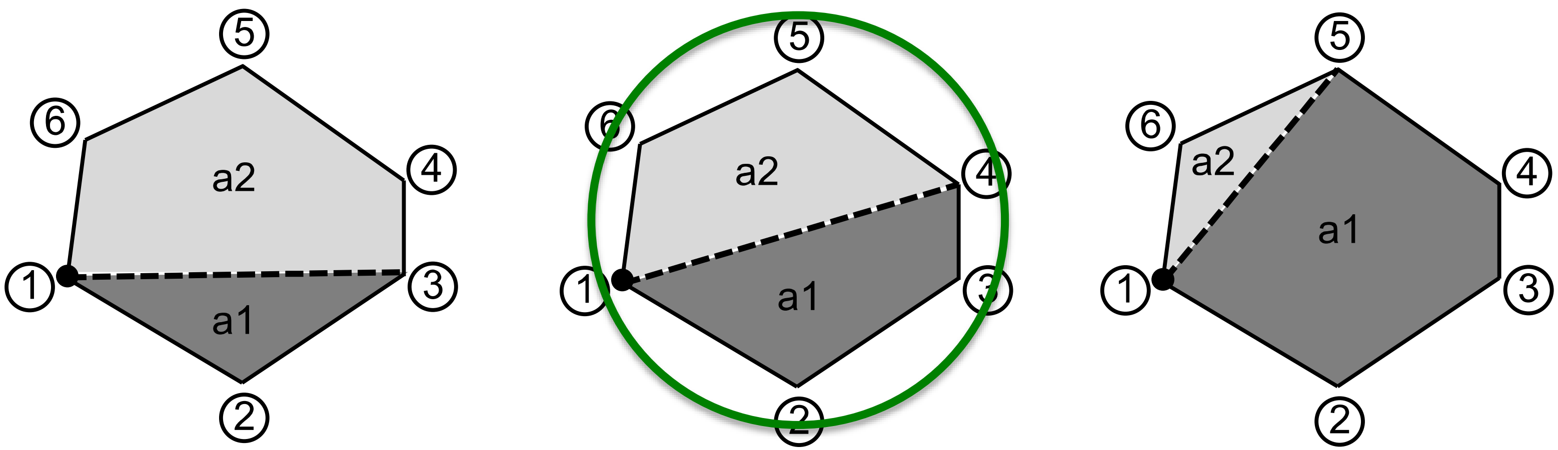

Element splitting decreases the error in crack length

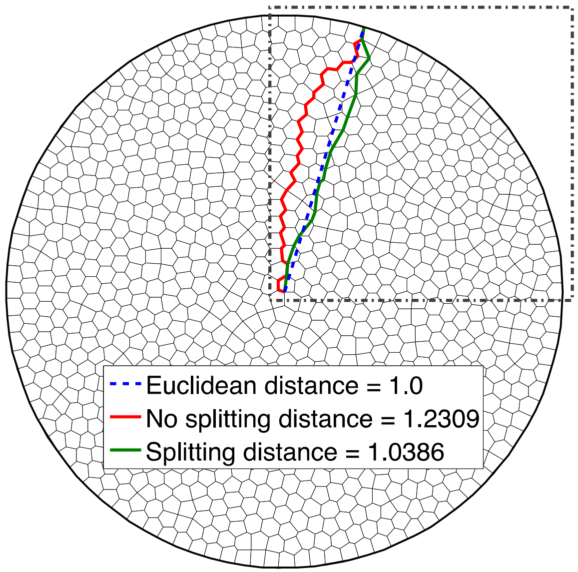

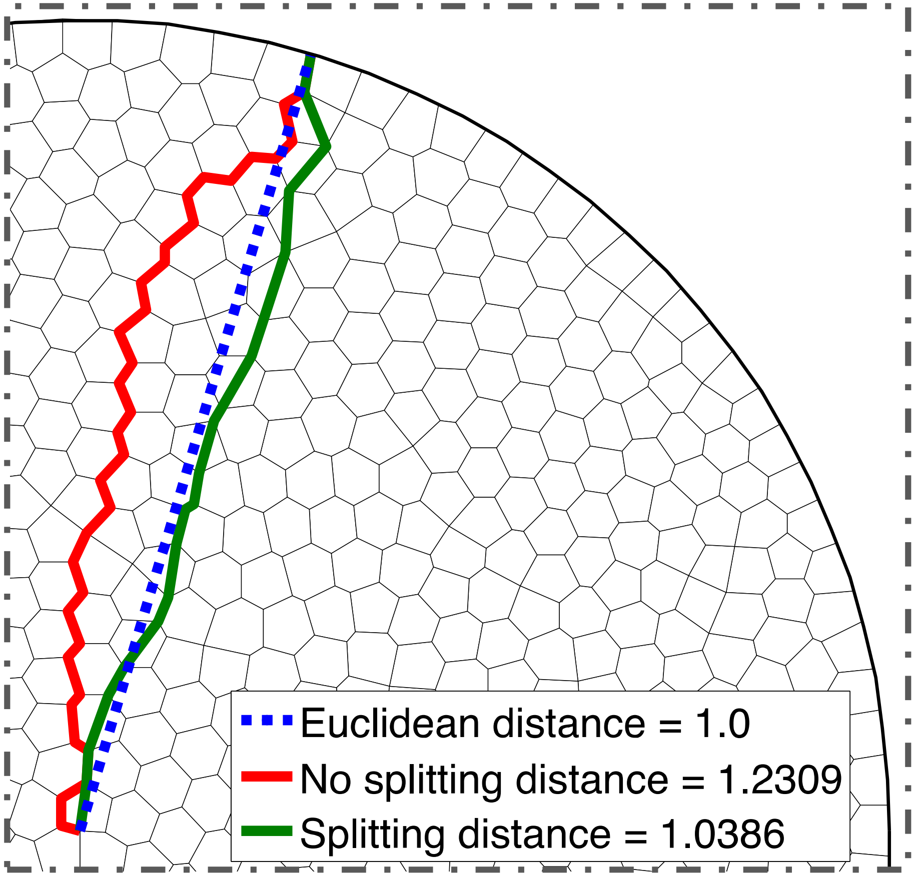

Element splitting decreases the error in crack length

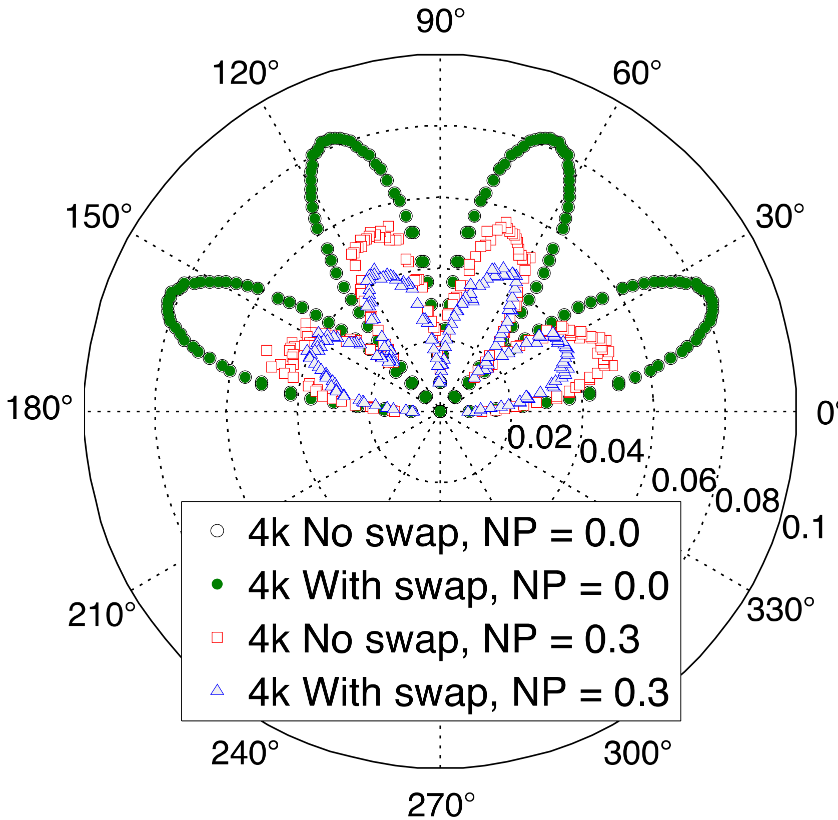

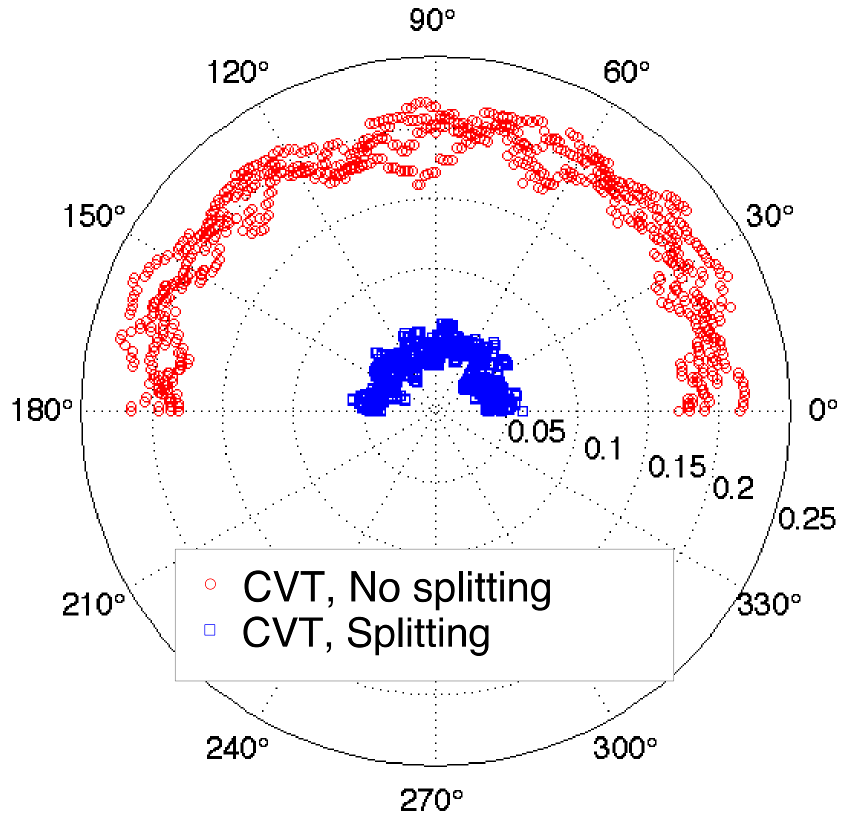

Element splitting preserves isotropy and reduced error significantly

Simple refinement strategies can be implemented on polygonal element meshes

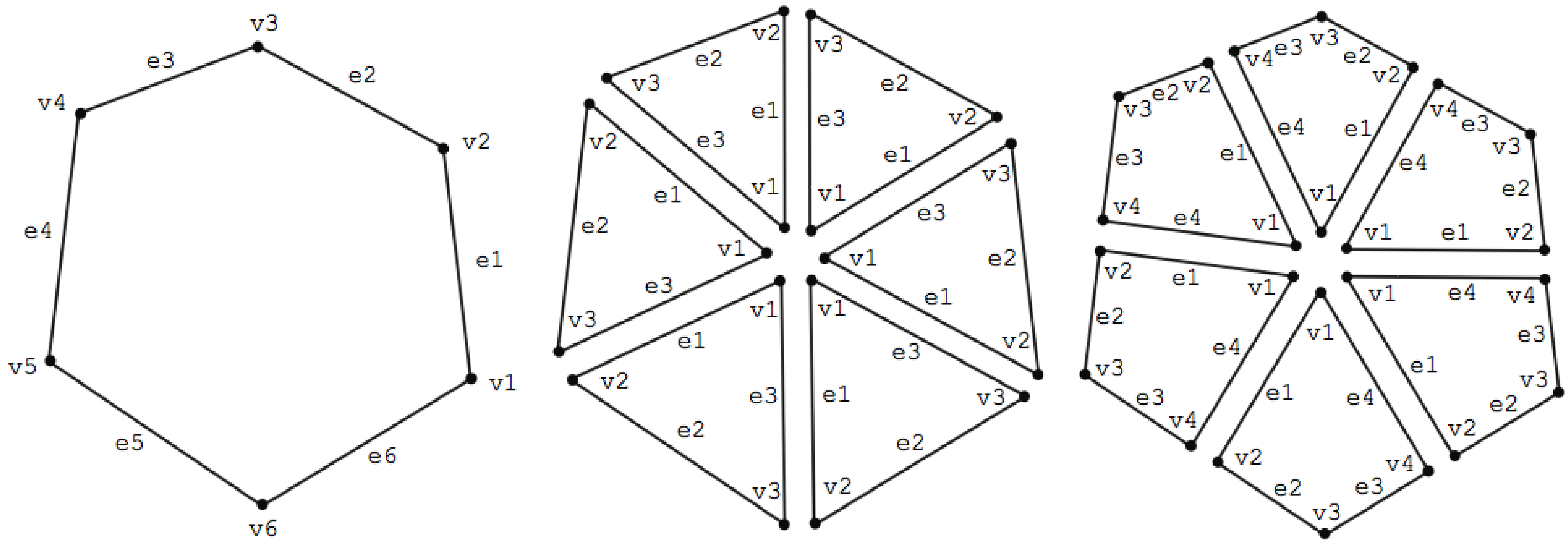

Spring, D. W., Leon, S. E., & Paulino, G. H., To be submitted to *IJNME*

In fracture simulation, crack tips are tracked and elements within a given radius are refined

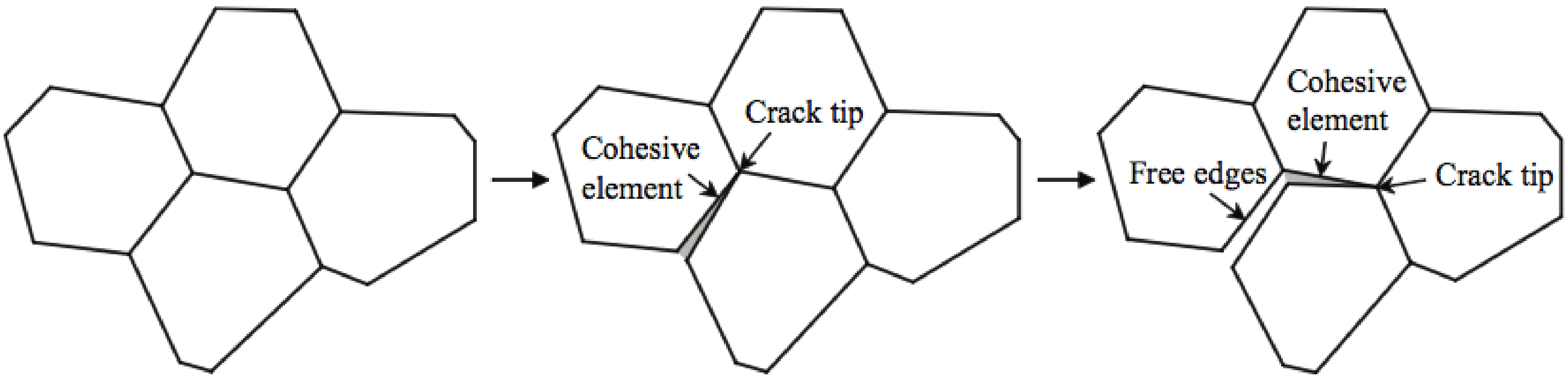

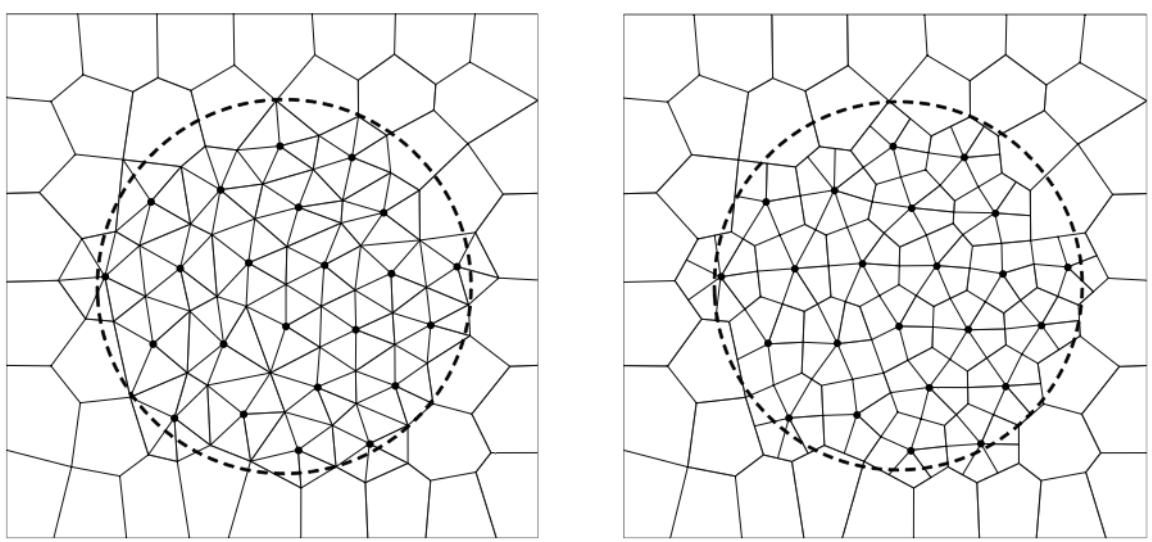

In the quad refinement scheme, “hanging nodes” are handled naturally

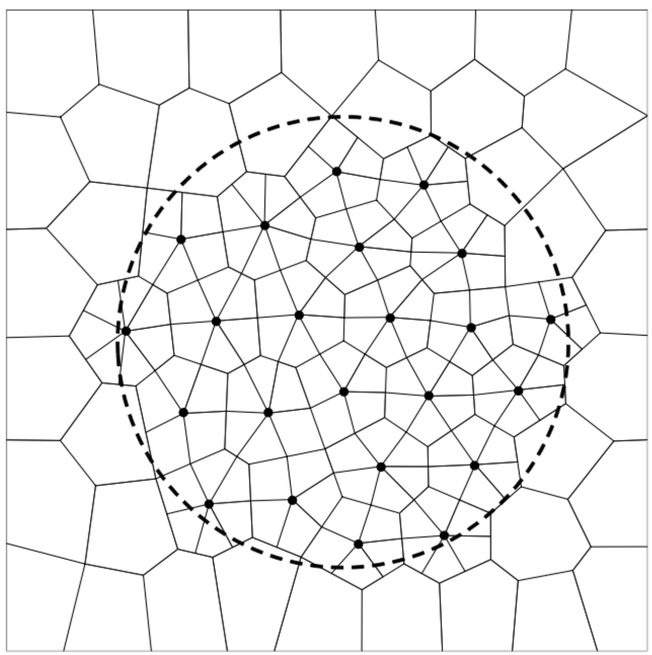

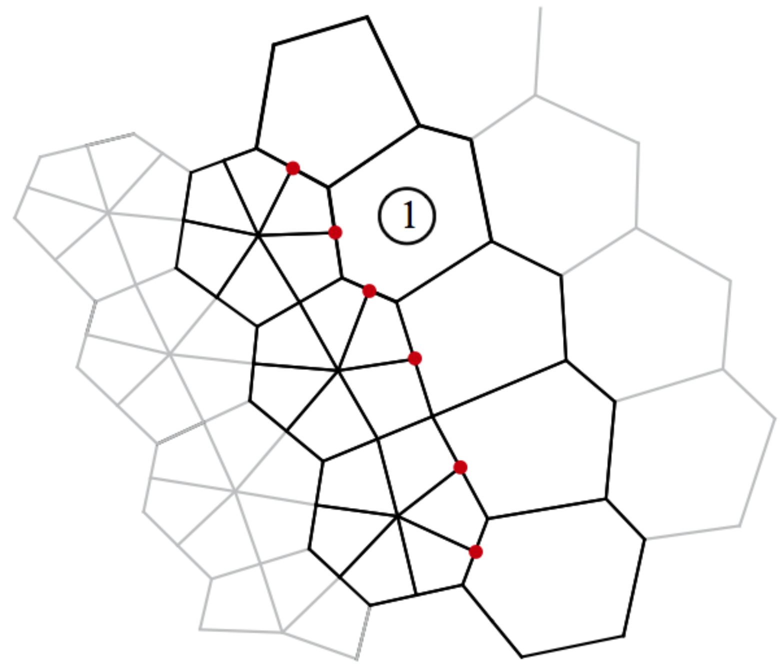

Before refinement: 6-sided polygon

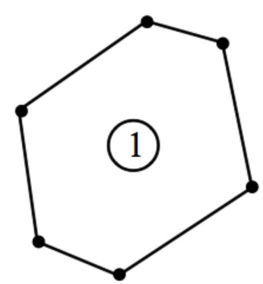

After refinement: 8-sided polygon

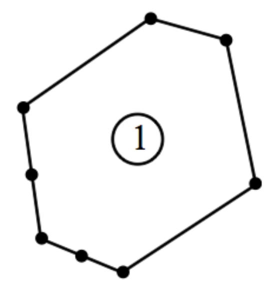

The error in crack length decreases when the mesh is refined

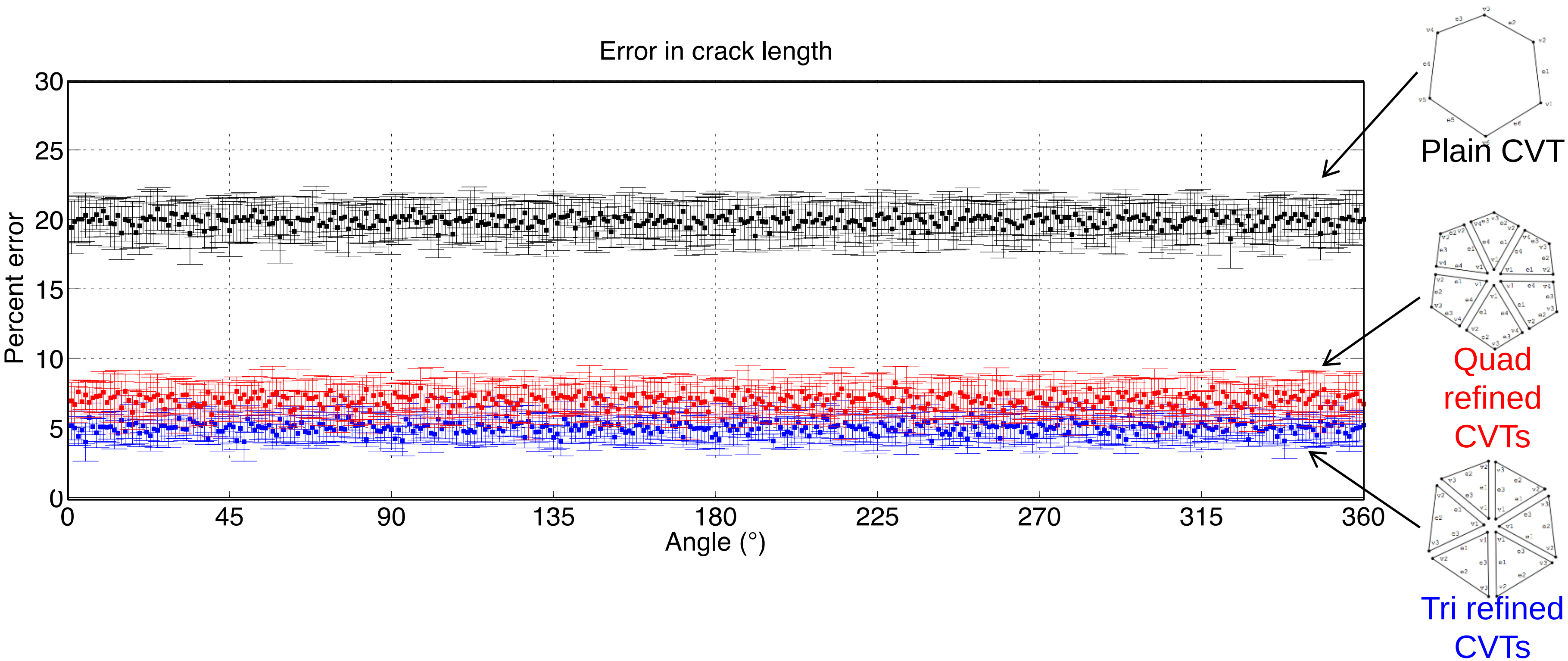

We want to take advantage of the splitting scheme, in which the error in crack length was between 3-5%

Element splitting plus quad refinement increases the number of potential crack directions

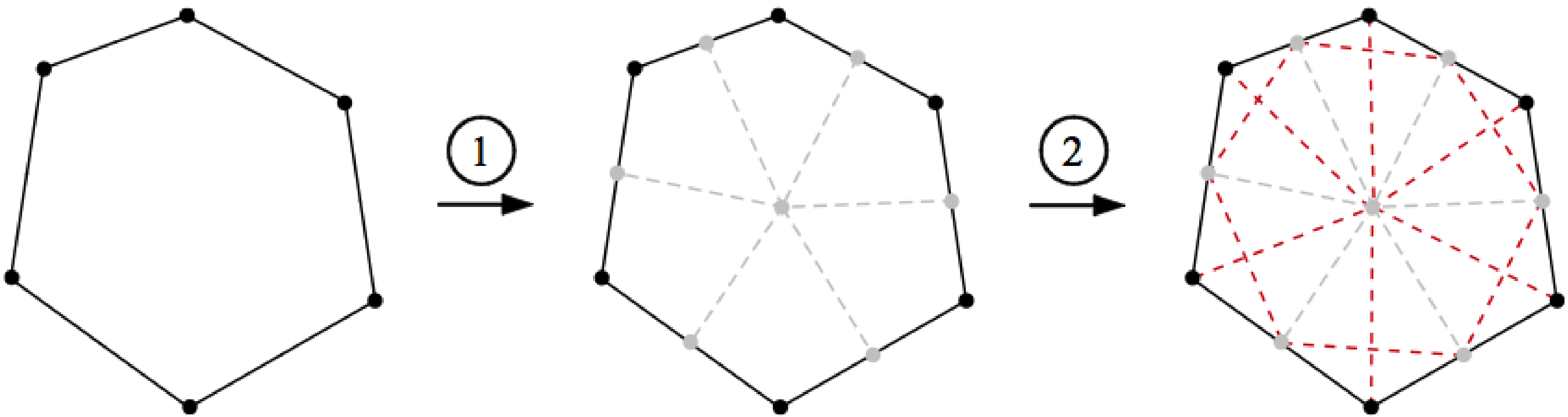

When element splitting is combined with quad refinement, the crack length error is very low

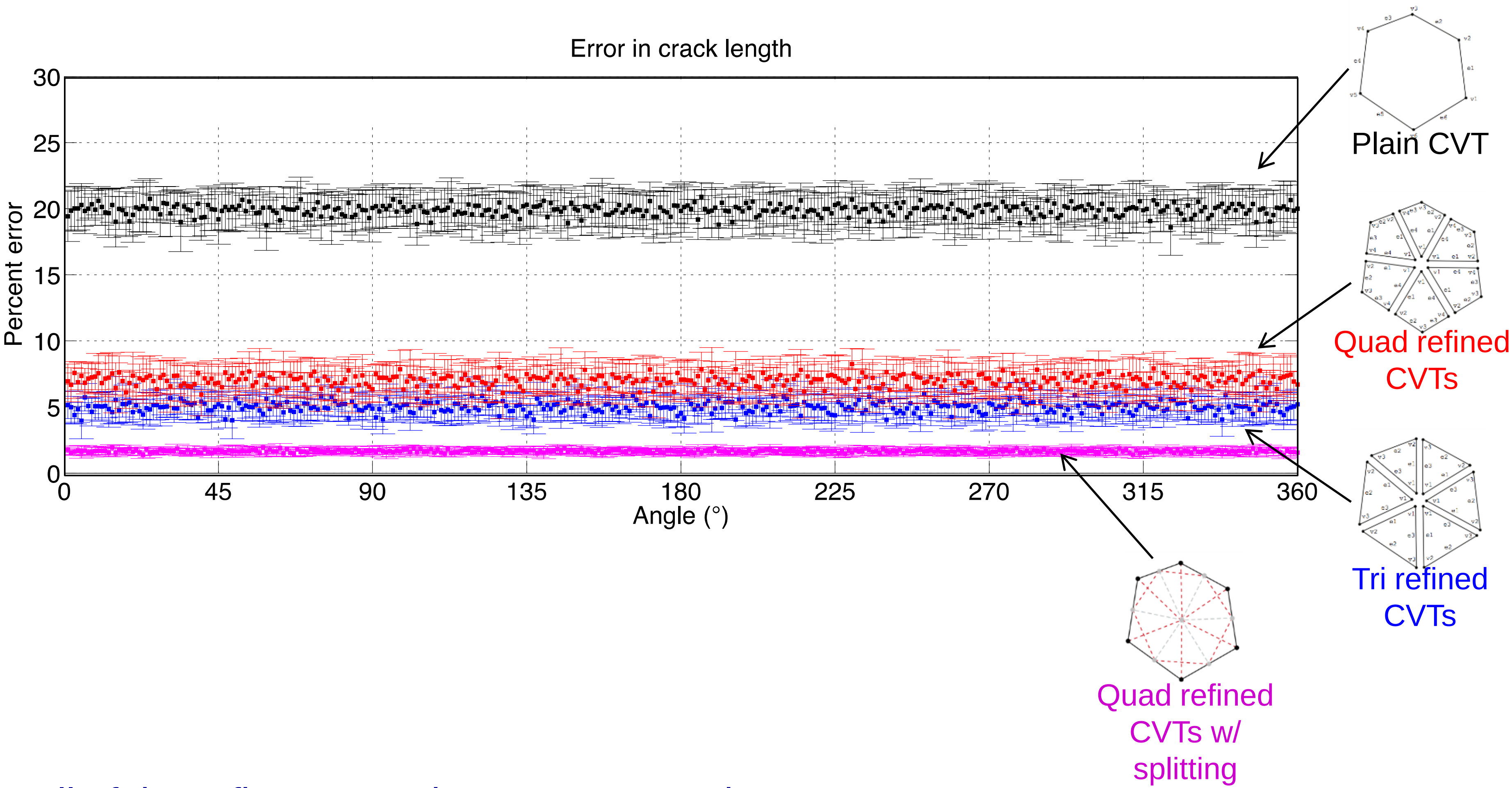

All of the refinement schemes preserve isotropy

Additional steps are performed to add new nodes and elements to the model

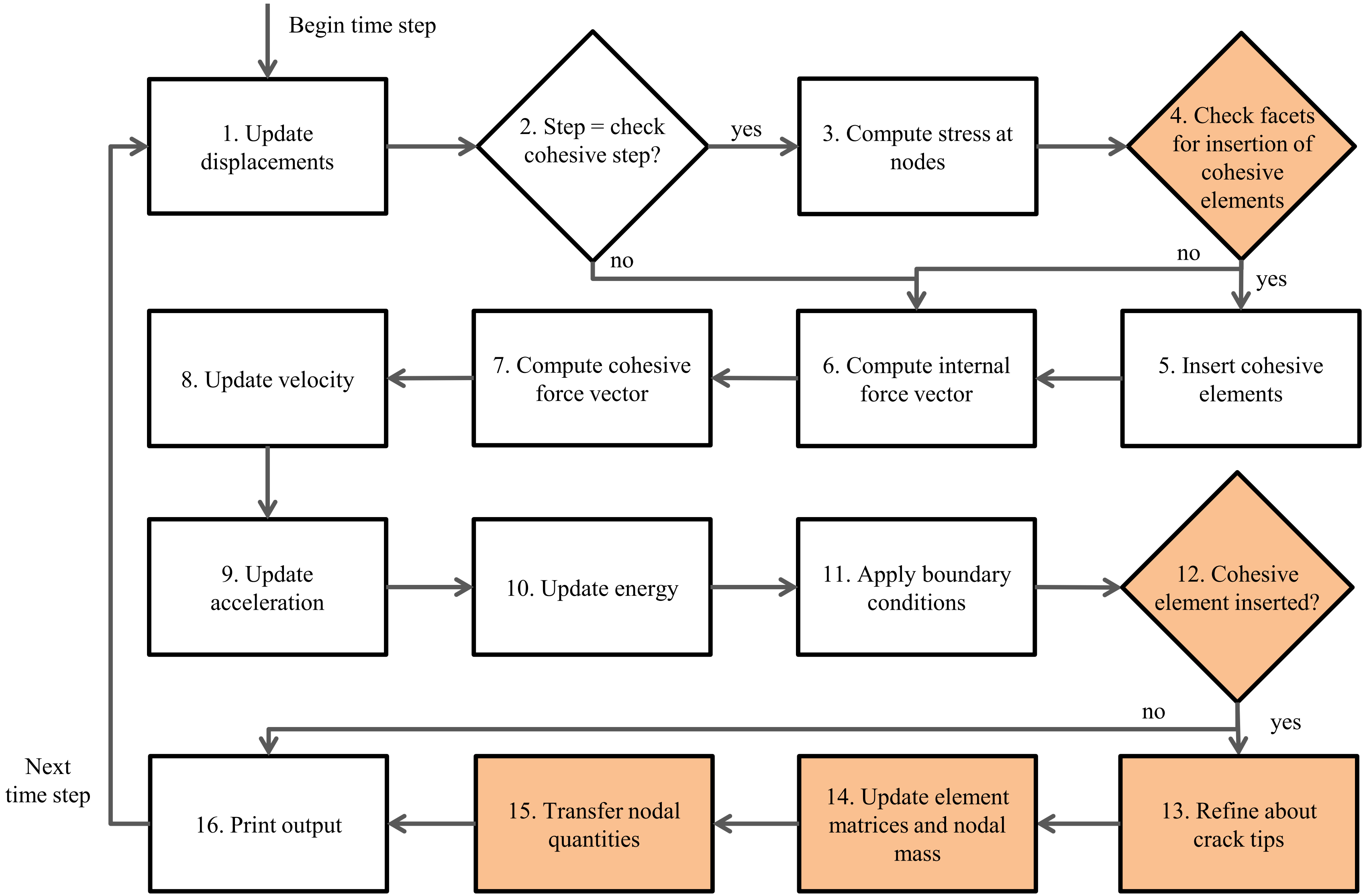

We employ a topological data structure, TopS, that makes on-the-fly mesh adaptation efficient

Implicit and explicit entities enabled mesh modification operators to occur in linear time

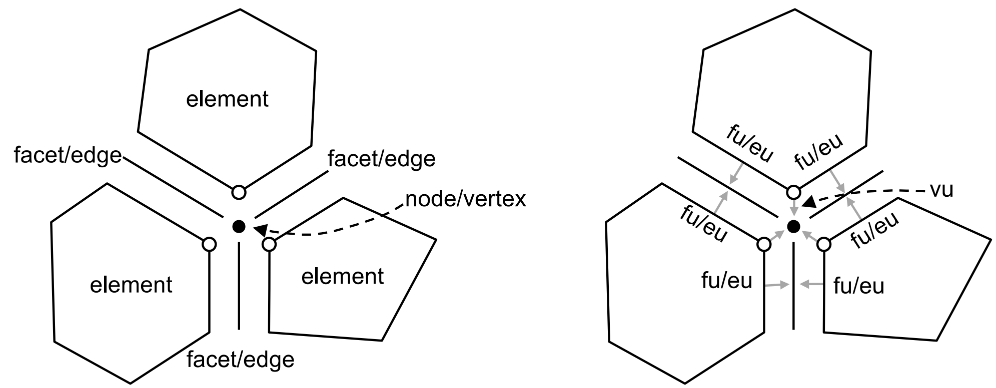

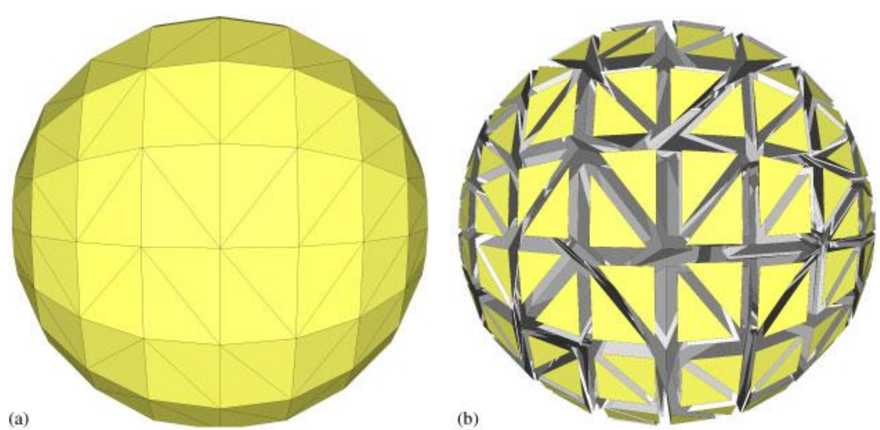

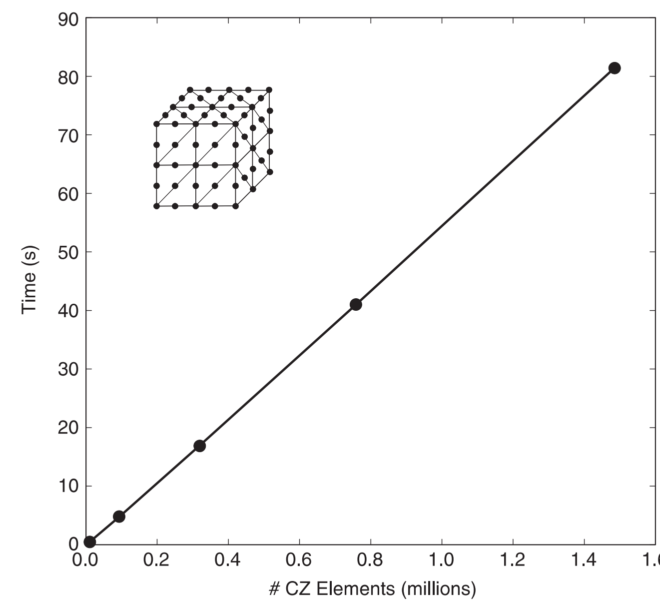

Celes, W., Paulino, G. H., & Espinha, R. *IJNME*, 64(11) 1529–1556, 2005.
Celes, W., Paulino, G.H., & Espinha, R. *Journal of Computing and Information Science in Engineering,* 5(4) , 2005.

Dynamic fracture with element splitting results in desired crack patterns

Compact Compression Specimen investigated with polygonal elements and splitting

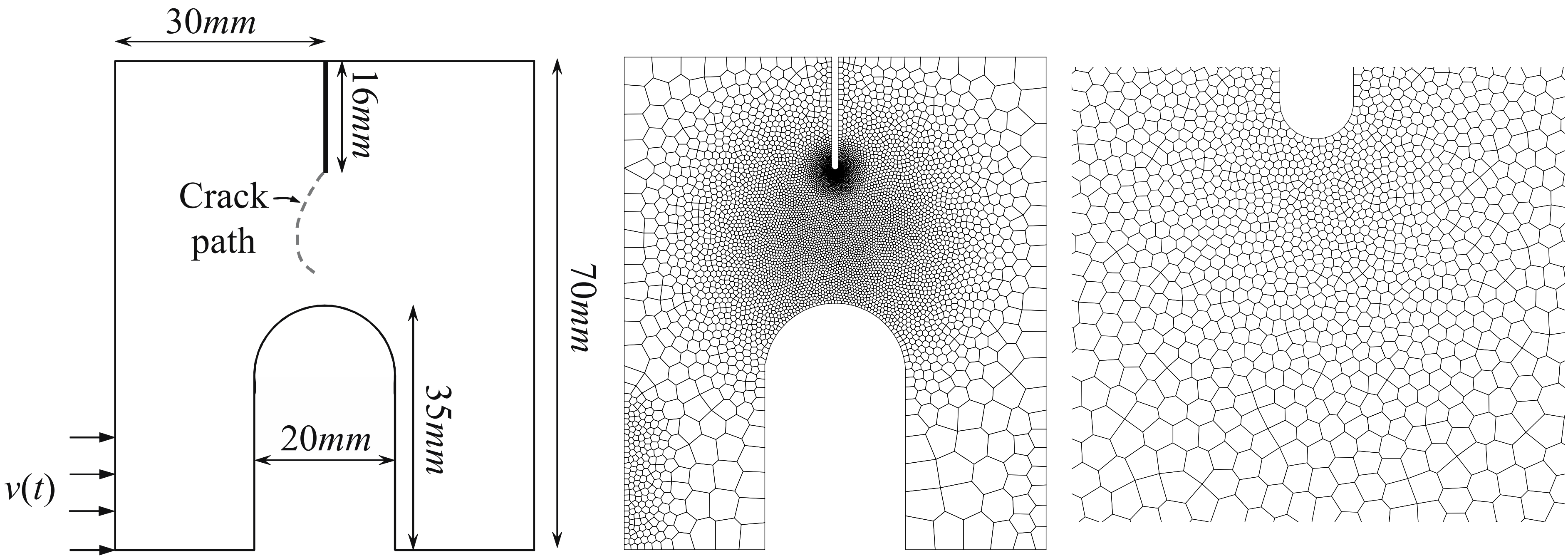

Rittel D, Maigre H. *Mechanics of Materials,* 23(3), 229–239, 1996.

Polygonal elements with splitting provide excellent results for CCS test

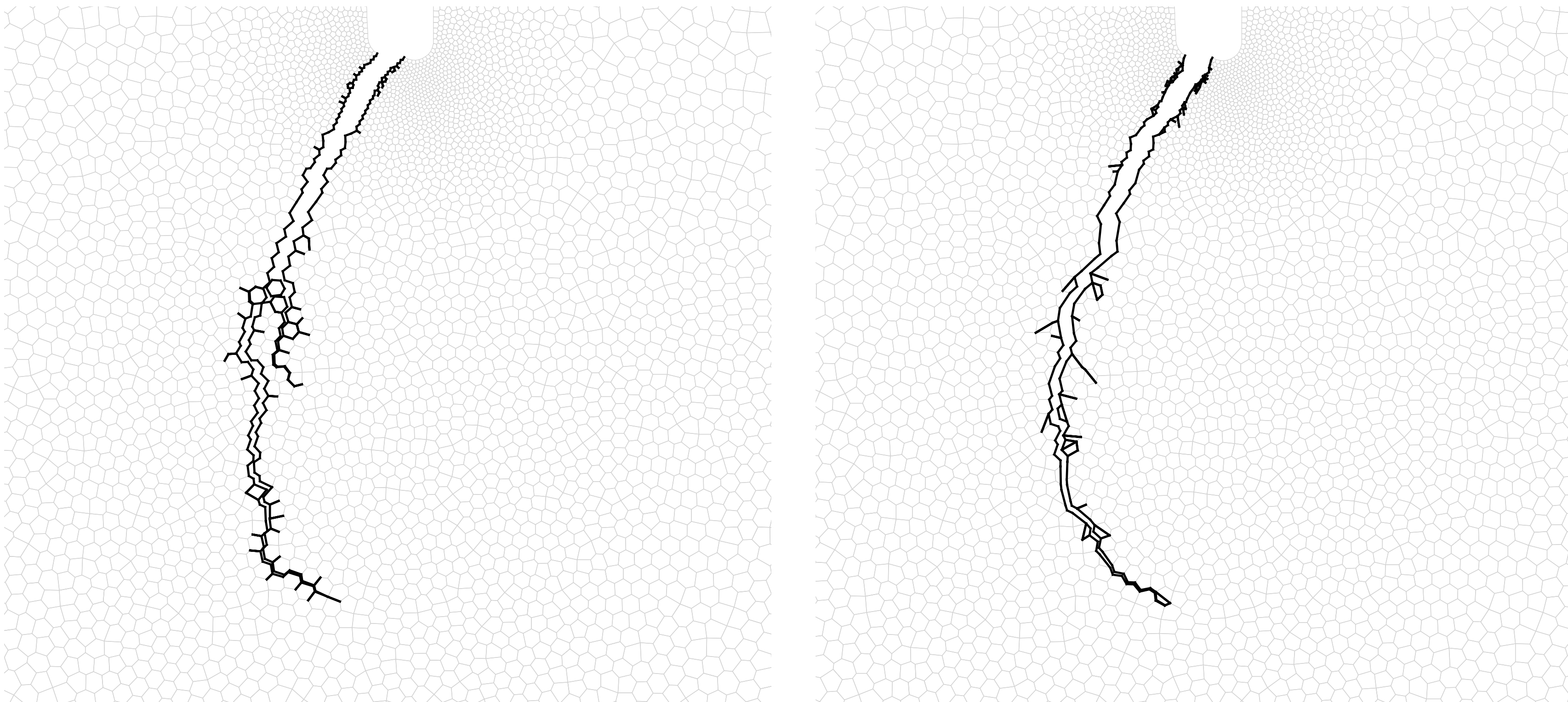

Polygonal elements with splitting provide excellent results for CCS test

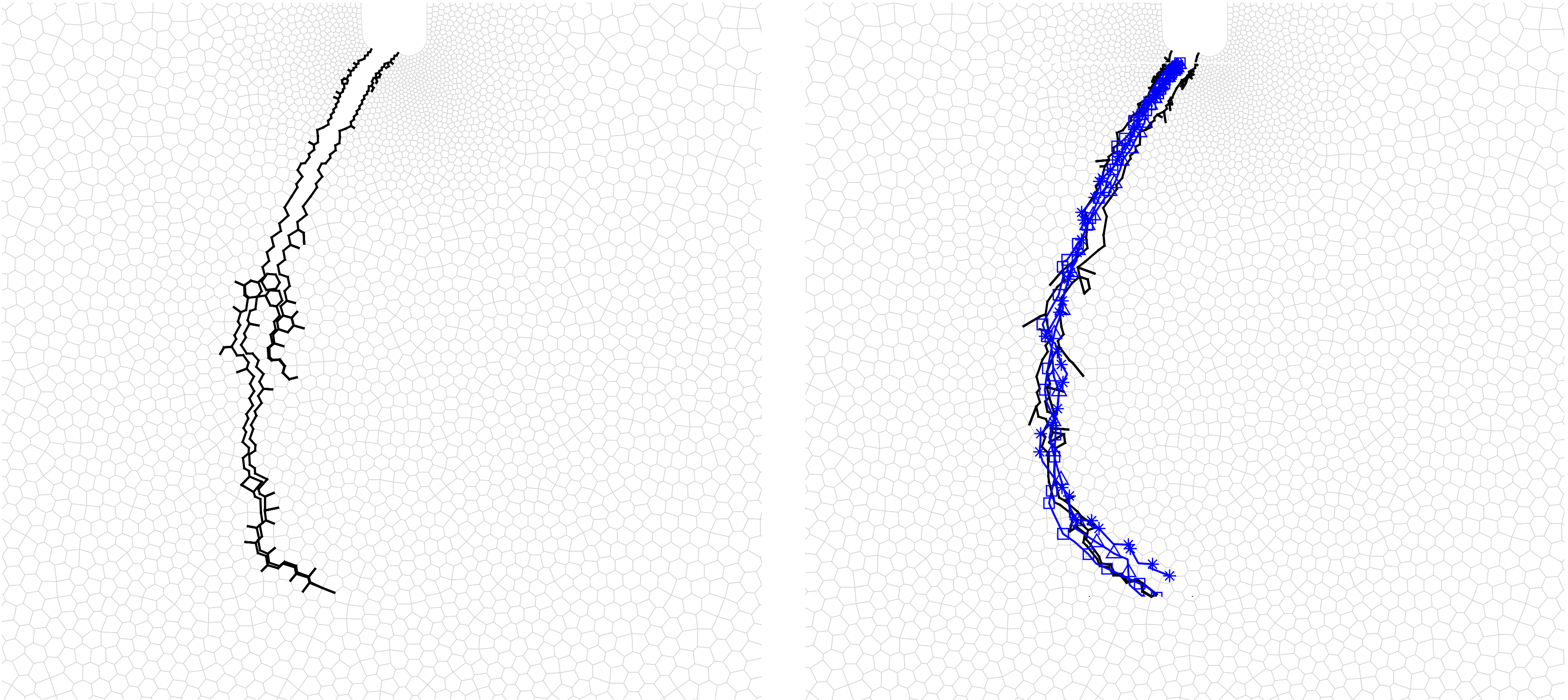

Papoulia, K. D., Vavasis, S. A., & Ganguly, P. *IJNME*, 67(1), 1–16, 2006.

Desirable results are obtained with mesh refinement while reducing computational cost

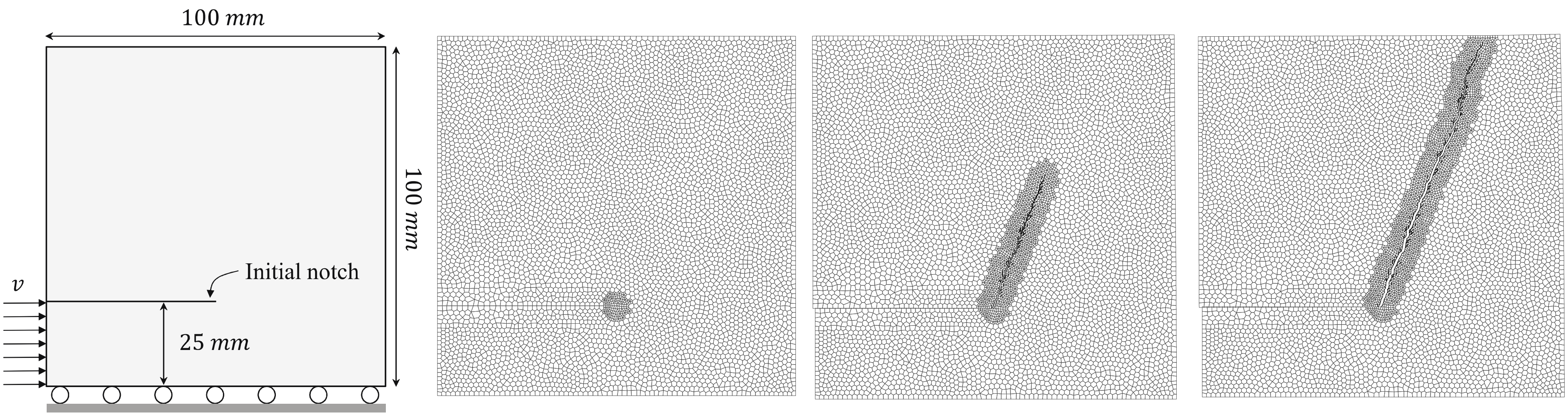

Mesh refinement is performed as needed in time (Case 3)

Case	Wall time (min)
(1) ~33,000 CVT polygons (60,314 Nodes)	141.7
(2) 6,000 CVT polygons refined = ~33,000 elements (33,629 Nodes)	89.8
(3) 6000 CVT polygons with adaptive refinement (10,815 Nodes)	25.3

Kalthoff JF, Winkler S. *International Conference on Impact Loading and Dynamic Behavior of Materials*, Bremen, Germany, vol. 1, 185–195, 1987.

Quadrilateral refinement plus splitting is superior than individual schemes

Full test specimen

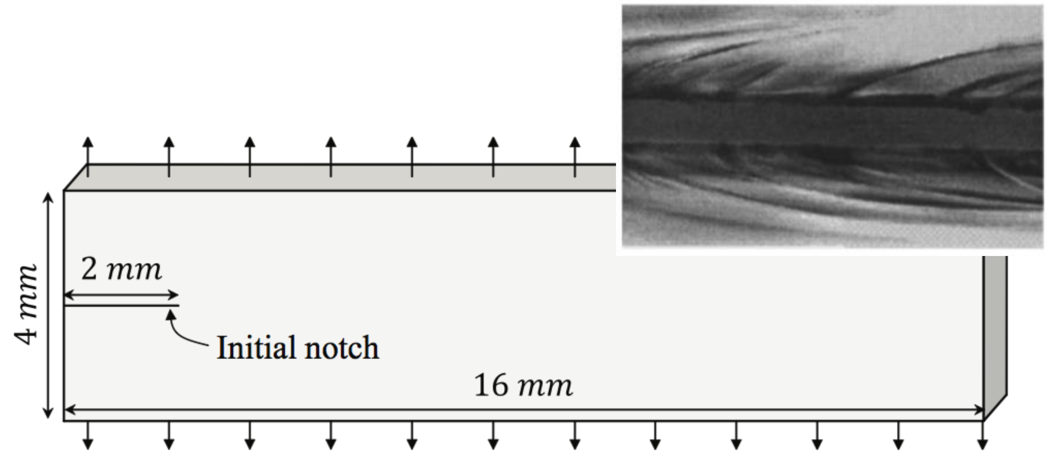

Polygonal elements only

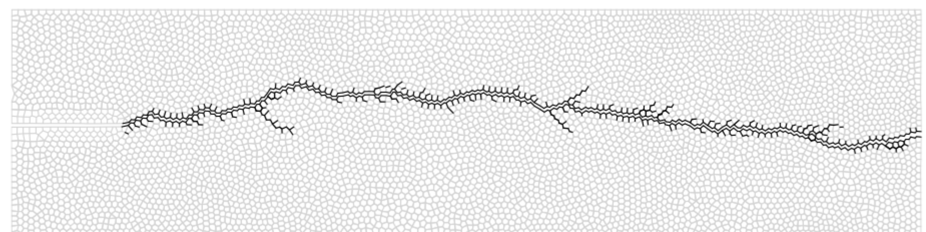

Refinement + element splitting

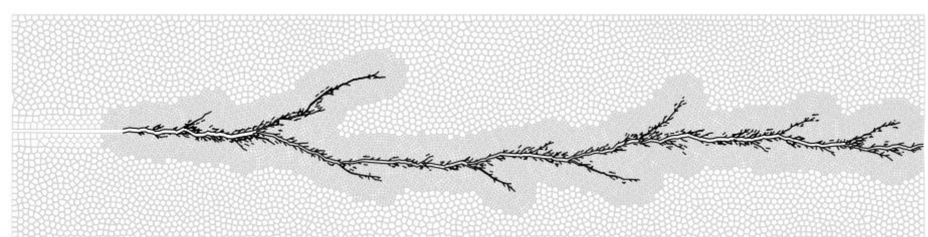

Sharon, E., & Fineberg, J. *Physical Review B.* 54(10), 7128–7139, 1996.

Some concluding remarks

- Inter-element cohesive zone modeling provides a means to capture the complex nonlinear behavior at a crack tip
- Polygonal finite elements are well suited for fracture simulation as they do not impart bias on the crack patterns
- With the help of a topological data structure and an explicit time integration scheme, mesh adaptation can be performed on-the-fly to allow for improved results with reduced computational effort

Some concluding remarks

- Inter-element cohesive zone modeling provides a means to capture the complex nonlinear behavior at a crack tip
- Polygonal finite elements are well suited for fracture simulation as they do not impart bias on the crack patterns
- With the help of a topological data structure and an explicit time integration scheme, mesh adaptation can be performed on-the-fly to allow for improved results with reduced computational effort

Questions?

Back up slides

Many models exist in the literature, and PPR parameters can be tuned to recover them

PPR
$\alpha = \beta = 5$
$\delta_n = 0.13$
$\delta_t = 0.1$
$\Phi_n = \Phi_t = 352.3$ J/m^2
$\sigma = 324$ MPa
$\tau = 755.4$ MPa

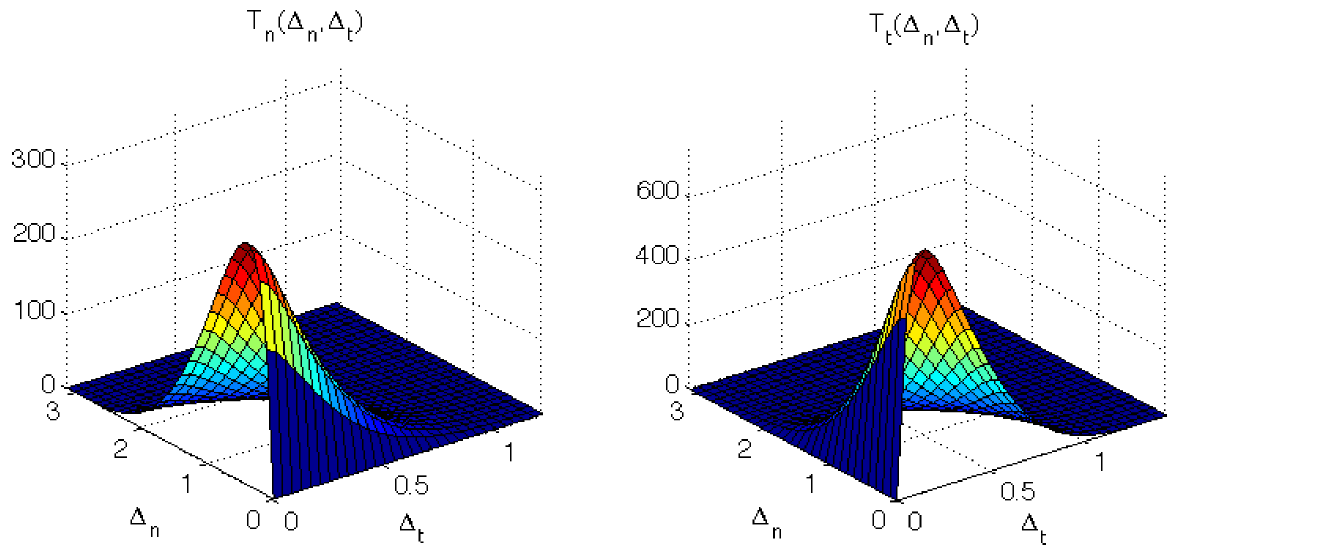

Xu and Needleman 1994
$r = 0$
$\delta_{cn} = 0.4\mu m$
$\delta_{ct} = 0.4\mu m$
$\Phi_n = \Phi_t = 352.3$ J/m^2
$\sigma = 324$ MPa
$\tau = 755.4$ MPa

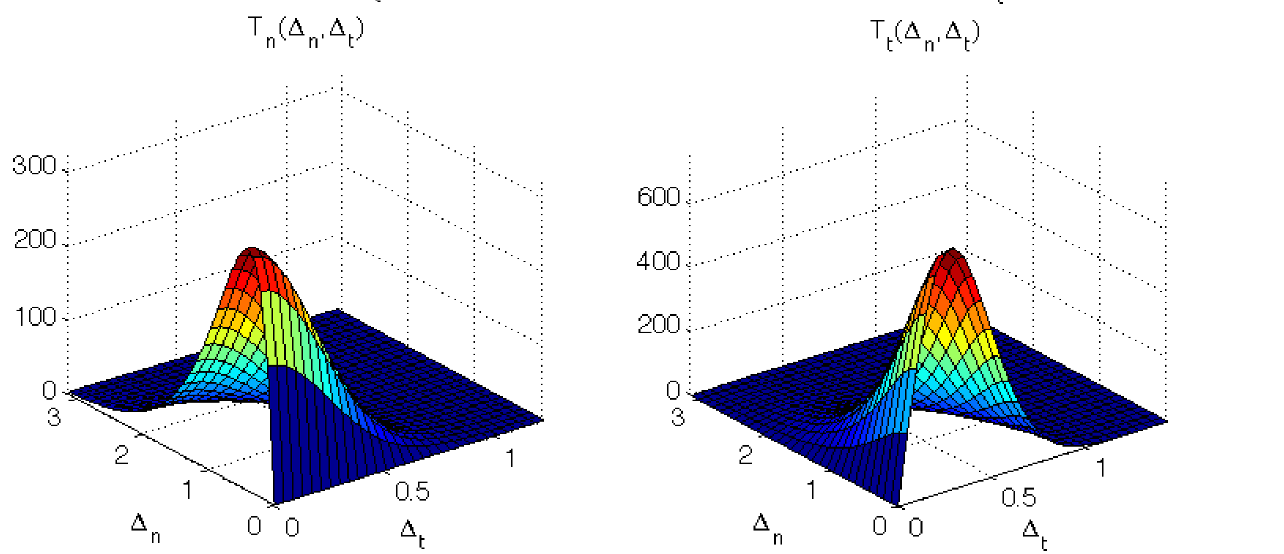

Park, K., Paulino, G. H., & Roesler, J. R. (2009). Journal of the Mechanics and Physics of Solids, 57(6), 891–908.
Xu, X.-P., & Needleman, A. (1994). *Journal of the Mechanics and Physics of Solids*, *42*(9).

The traction-separation relation is given by the PPR potential-based cohesive zone model

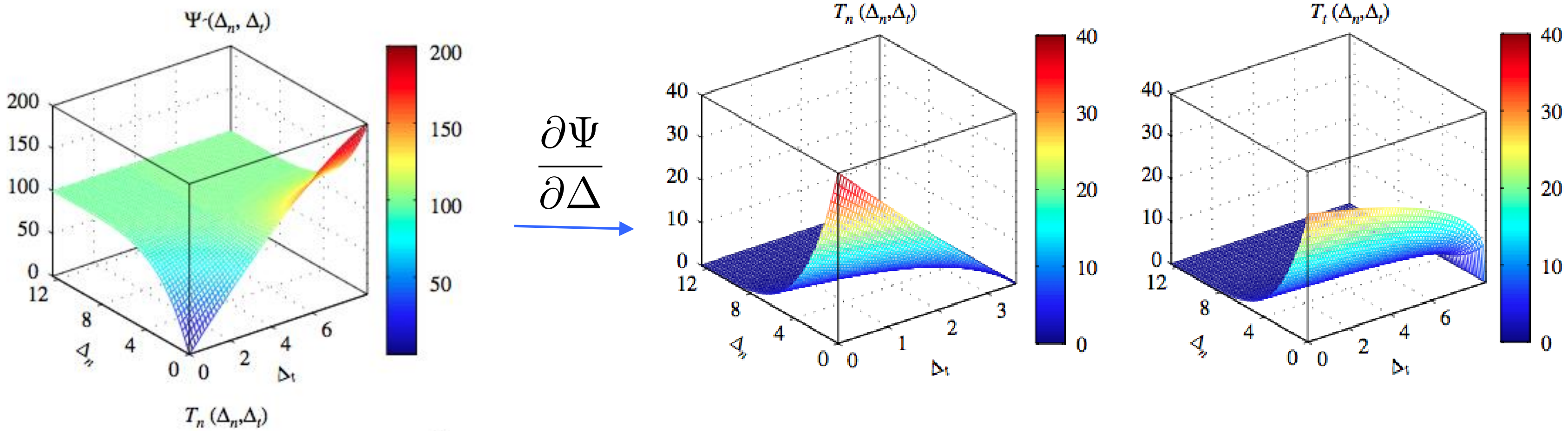

$$\Psi\left(\Delta_n, \Delta_t\right) = \min\left(\phi_n, \phi_t\right) + \left[\Gamma_n\left(1 - \frac{\Delta_n}{\delta_n}\right)^{\alpha} + \langle \phi_n - \phi_t \rangle\right]\left[\Gamma_t\left(1 - \frac{|\Delta_t|}{\delta_t}\right)^{\beta} + \langle \phi_t - \phi_n \rangle\right]$$

$$T_n\left(\Delta_n, \Delta_t\right) = -\alpha\frac{\Gamma_n}{\delta_n}\left(1 - \frac{\Delta_n}{\delta_n}\right)^{\alpha-1}\left[\Gamma_t\left(1 - \frac{|\Delta_t|}{\delta_t}\right)^{\beta} + \langle \phi_t - \phi_n \rangle\right]$$

$$T_t\left(\Delta_n, \Delta_t\right) = -\beta\frac{\Gamma_t}{\delta_t}\left(1 - \frac{|\Delta_t|}{\delta_t}\right)^{\beta-1}\left[\Gamma_n\left(1 - \frac{\Delta_n}{\delta_n}\right)^{\alpha} + \langle \phi_n - \phi_t \rangle\right]\frac{\Delta_t}{|\Delta_t|}$$

Extrinsic elements are inserted based on an external criteria when and where they are need, thus there is no initial slope

Park, K., Paulino, G. H., & Roesler, J. R. *JMPS*, 57(6), 891–908, 2009.

The traction-separation relation is given by the PPR potential-based cohesive zone model

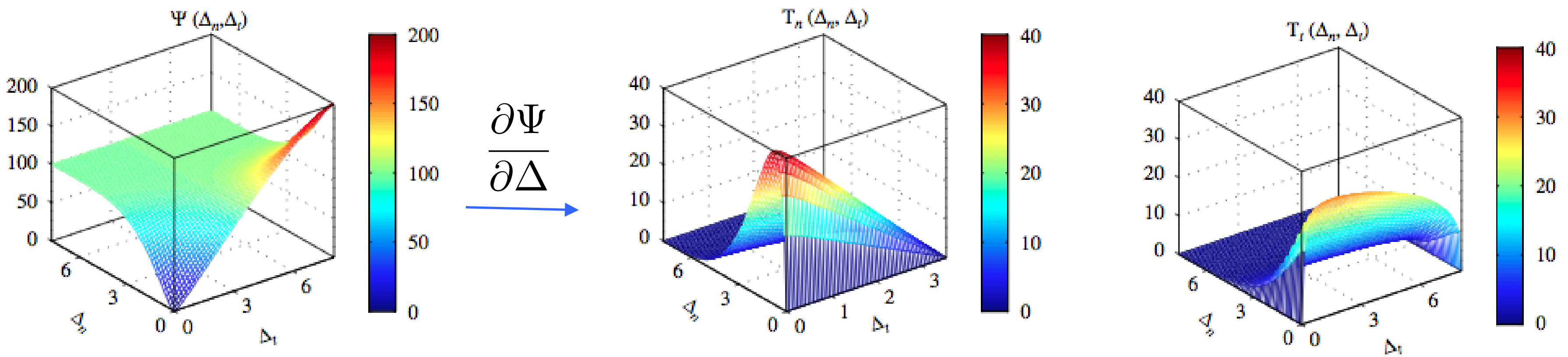

$$\Psi\left(\Delta_n,\Delta_t\right)=\min\left(\phi_n,\phi_t\right)+\left[\Gamma_n\left(1-\frac{\Delta_n}{\delta_n}\right)^{\alpha}\left(\frac{m}{\alpha}+\frac{\Delta_n}{\delta_n}\right)^{\alpha}+\langle\phi_n-\phi_t\rangle\right]\left[\Gamma_t\left(1-\frac{|\Delta_t|}{\delta_t}\right)^{\beta}\left(\frac{n}{\beta}+\frac{|\Delta_t|}{\delta_t}\right)^{n}+\langle\phi_t-\phi_n\rangle\right]$$

$$\begin{aligned}T_n\left(\Delta_n,\Delta_t\right)=&\frac{\Gamma_n}{\delta_n}\left[m\left(1-\frac{\Delta_n}{\delta_n}\right)^{\alpha}\left(\frac{m}{\alpha}+\frac{\Delta_n}{\delta_n}\right)^{m-1}-\alpha\left(1-\frac{\Delta_n}{\delta_n}\right)^{\alpha-1}\left(\frac{m}{\alpha}+\frac{\Delta_n}{\delta_n}\right)^{m}\right]\\&\times\left[\Gamma_t\left(1-\frac{|\Delta_t|}{\delta_t}\right)^{\beta}\left(\frac{n}{\beta}+\frac{|\Delta_t|}{\delta_t}\right)^{n}+\langle\phi_t-\phi_n\rangle\right]\end{aligned}$$

$$\begin{aligned}T_t\left(\Delta_n,\Delta_t\right)=&\frac{\Gamma_t}{\delta_t}\left[n\left(1-\frac{|\Delta_t|}{\delta_t}\right)^{\beta}\left(\frac{n}{\beta}+\frac{|\Delta_t|}{\delta_t}\right)^{n-1}-\beta\left(1-\frac{|\Delta_t|}{\delta_t}\right)^{\beta-1}\left(\frac{n}{\beta}+\frac{|\Delta_t|}{\delta_t}\right)^{n}\right]\\&\times\left[\Gamma_n\left(1-\frac{\Delta_n}{\delta_n}\right)^{\alpha}\left(\frac{m}{\alpha}+\frac{\Delta_n}{\delta_n}\right)^{m}+\langle\phi_n-\phi_t\rangle\right]\frac{\Delta_t}{|\Delta_t|}\end{aligned}$$

Intrinsic elements are present at the beginning of the simulation, thus an initial slope exists

Park, K., Paulino, G. H., & Roesler, J. R. *JMPS*, 57(6), 891–908, 2009.

CZ elements may be inserted *a priori* (intrinsic) or when/where they are needed (extrinsic)

Intrinsic approach is appropriate for scenarios where the crack propagation direction is known, e.g. material interfaces, but are not well suited for scenarios when the crack direction is unknown

Mesh topology does not change in an intrinsic scheme, but constantly changes in an extrinsic scheme

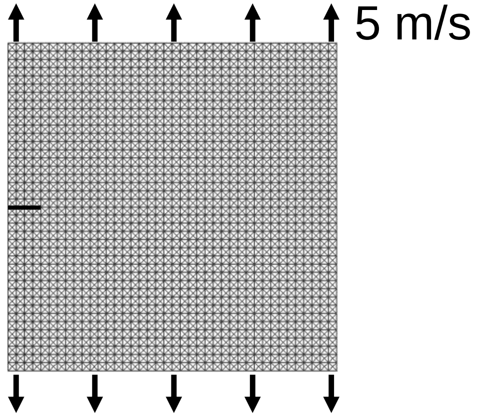

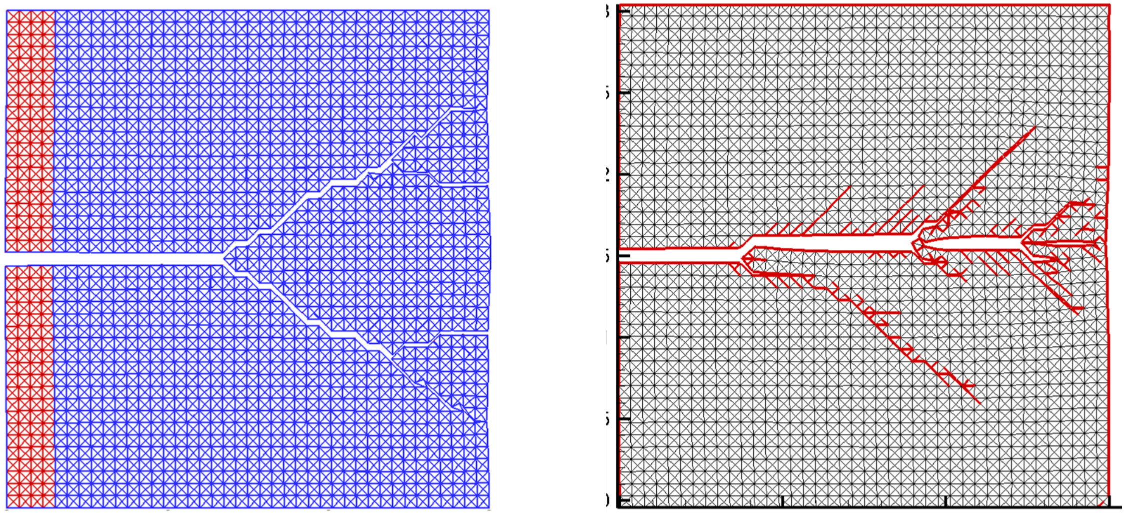

Hausdorff distances are also lower for polygonal meshes compared to 4k

Given a discretized path, P, whose vertices are p, and a mathematical path Q, the Hausdorff distance is

$$H(P, Q) = \max_{p \in P} \left[\min_{q \in Q} [\mathrm{dist}(p, q)] \right]$$

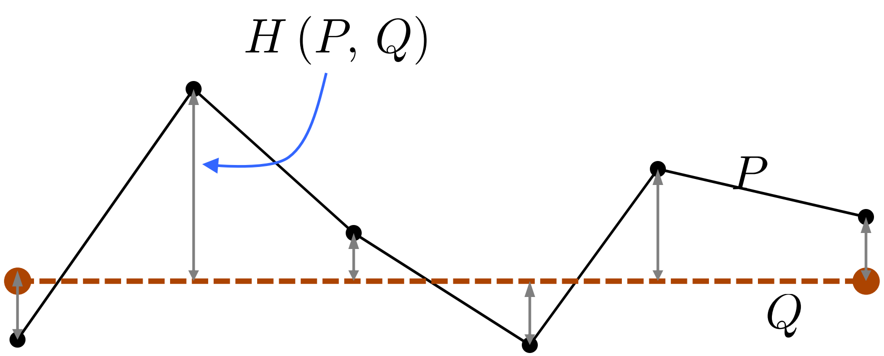

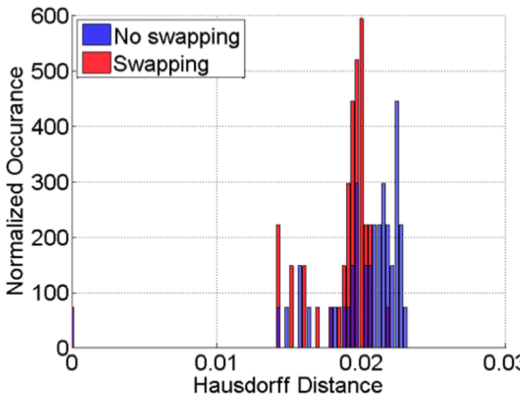

Unperturbed 4K

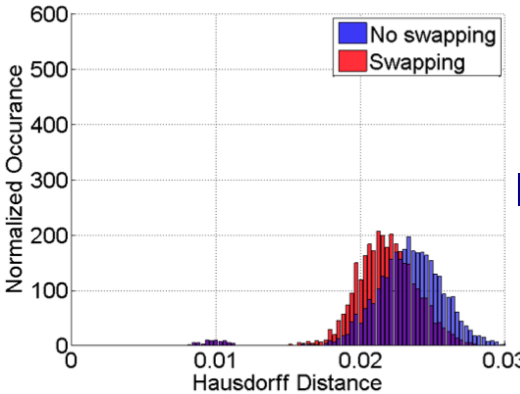

Perturbed 4K

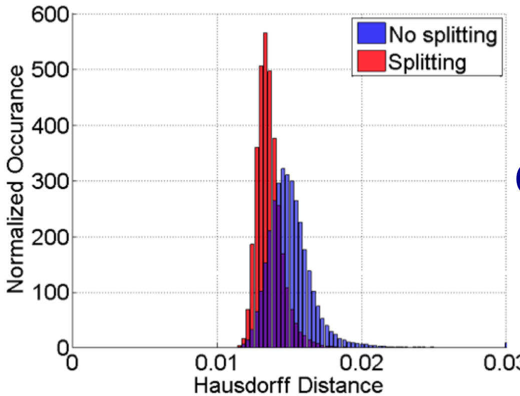

CVT

Quad refinement results in lower error for crack length studies

1,700 CVT elements
1,700 CVT element refined ~10,000 quads
~10,000 CVT elements

Without splitting

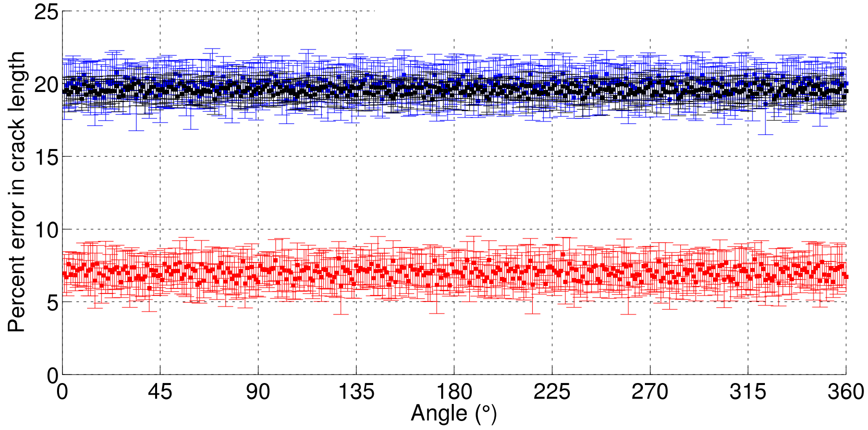

With splitting

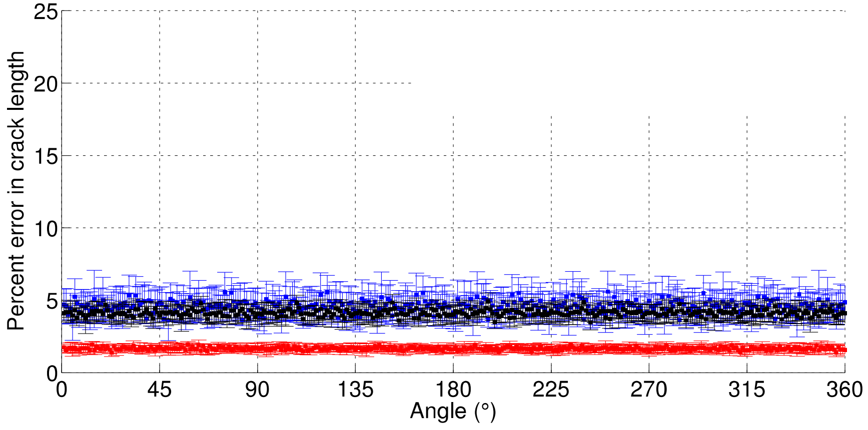

CVT element meshes that are refined with quads have lower error than meshes with an equivalent number of CVT elements.

Error in Hausdorff distance with refinement is nearly as low as a mesh of fine polygons

1,700 CVT elements
1,700 CVT element refined ~10,000 quads
~10,000 CVT elements

Without splitting

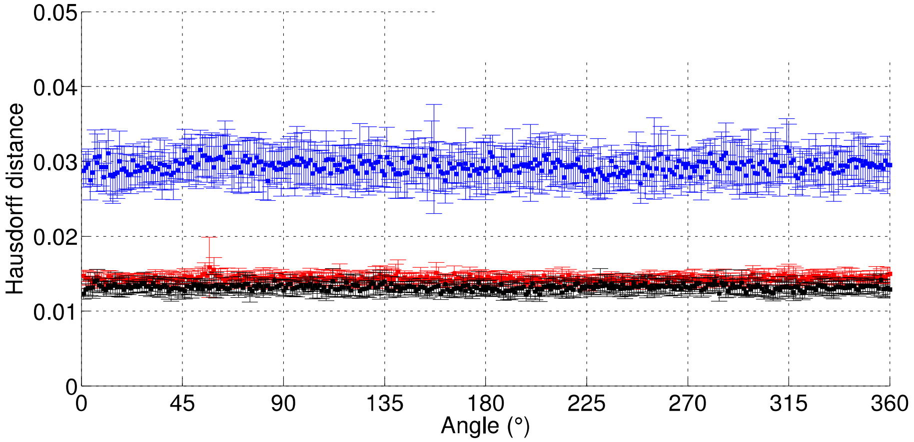

With splitting

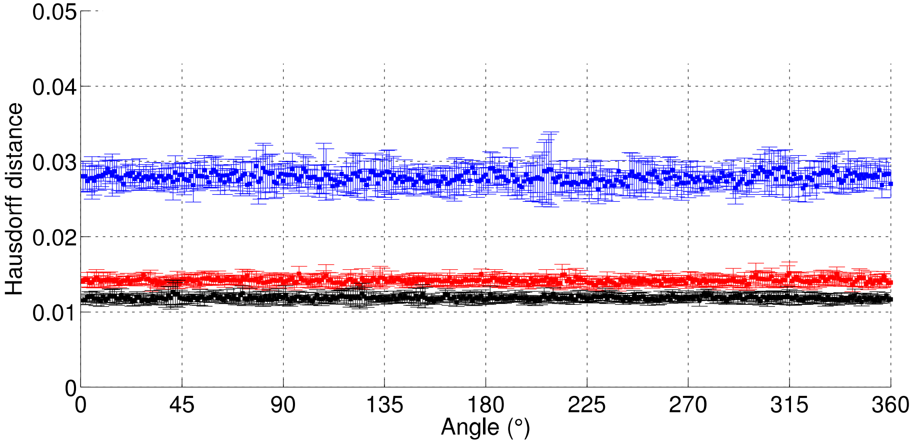

Since the proposed refinement scheme will be applied adaptively, we will gain the benefit of a smaller Hausdorff distance associated with using a fine mesh without needing to refine the entire domain.

We also perform studies on crack angle because it is a quantity of interest in fracture simulation

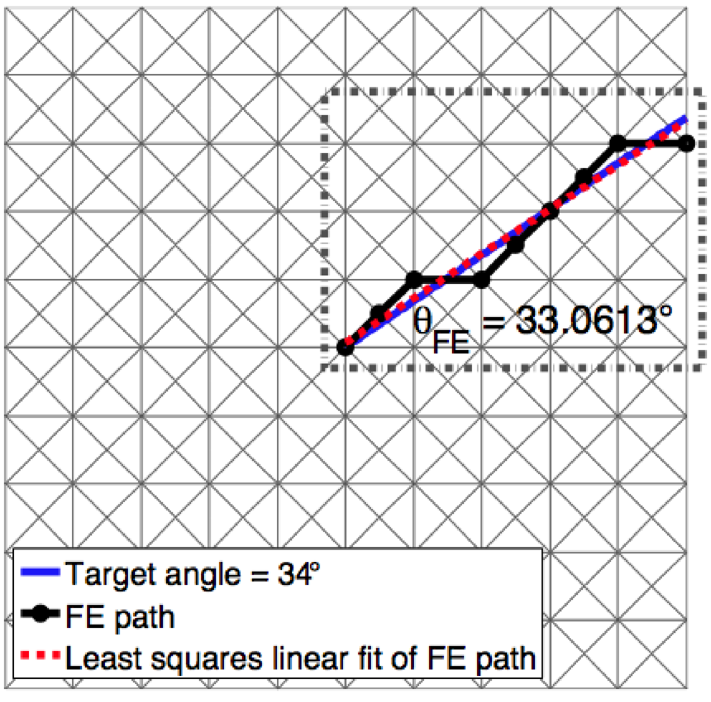

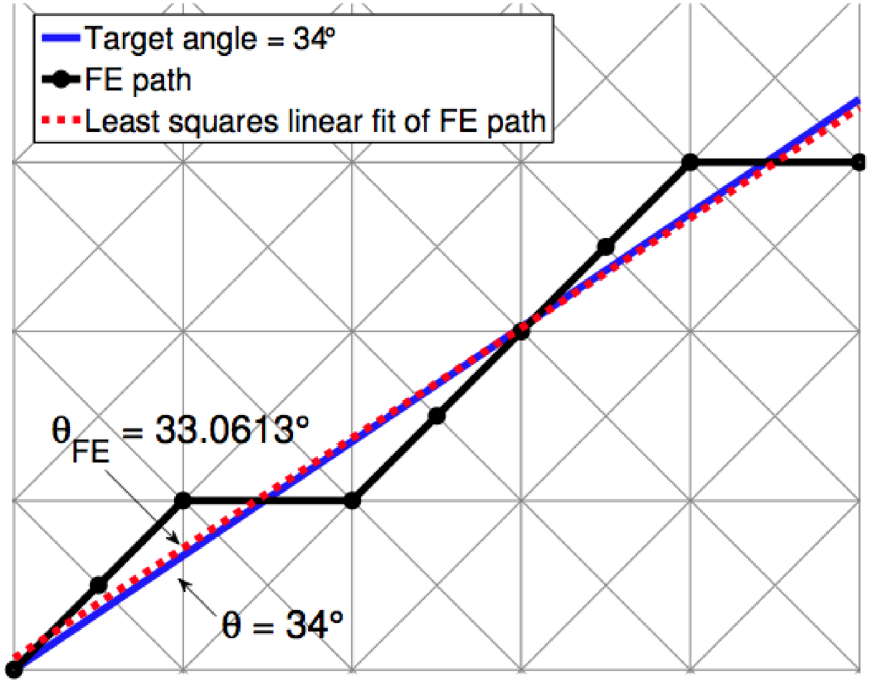

[Leon et al, 2013]

Crack angle deviation is significantly lower with polygonal meshes compared to 4K

No splitting/swapping

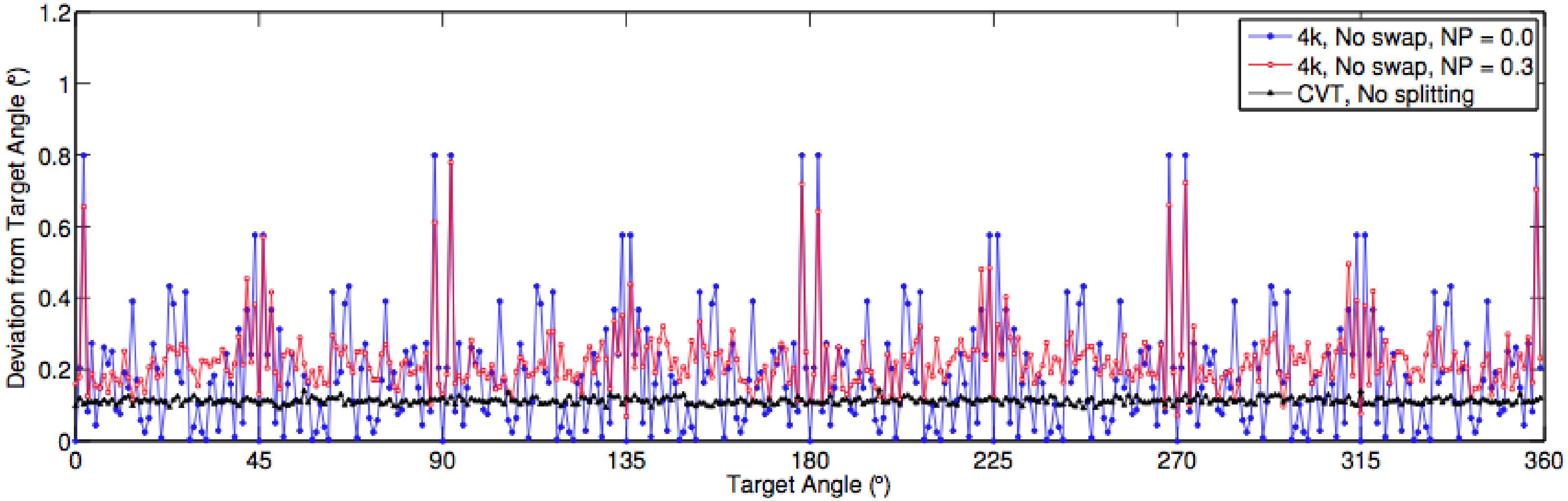

With splitting/swapping

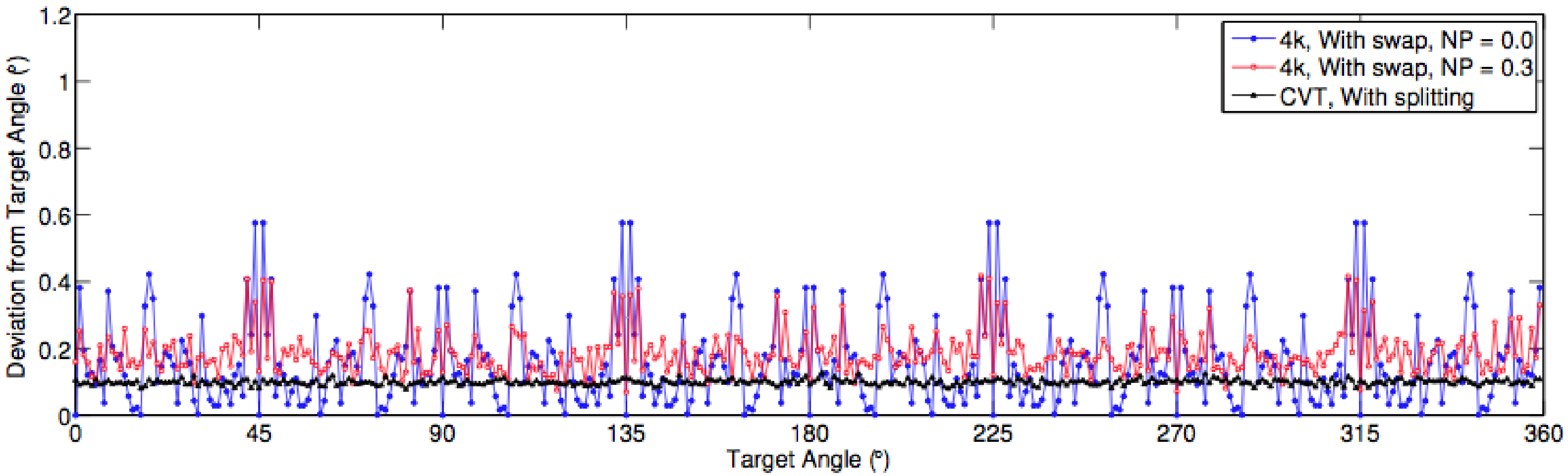

[Leon et al, 2013]

Instead of structured meshes, we use polygonal discretizations obtained from a Voronoi diagram

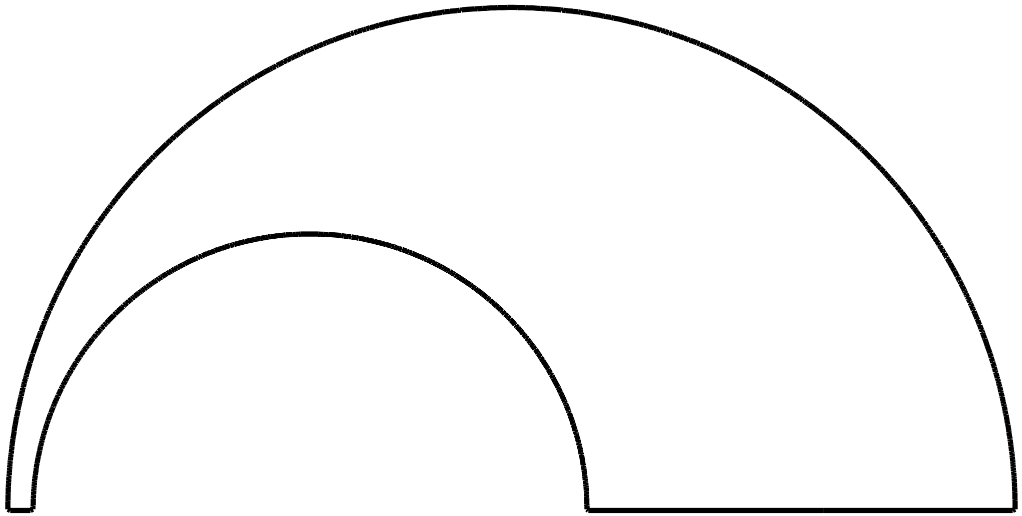

Voronoi tessellation associated with point set, P:

$$\mathcal{T}(\mathbf{P};\Omega) = \{V_{\mathrm{y}} \cap \Omega : \mathbf{y} \in \mathbf{P}\}$$

$$V_{\mathrm{y}} = \left\{\mathbf{x} \in \mathbb{R}^d : \|\mathbf{x}-\mathbf{y}\| < \|\mathbf{x}-\mathbf{z}\|, \forall \mathbf{z} \in \mathbf{P} \setminus \{\mathbf{y}\}\right\}$$

Voronoi cells

Talischi, C., Paulino, G. H., Pereira, A., & Menezes, I. F. M. *JSMO* 45(3), 309–328, 2012.

Instead of structured meshes, we use polygonal discretizations obtained from a Voronoi diagram

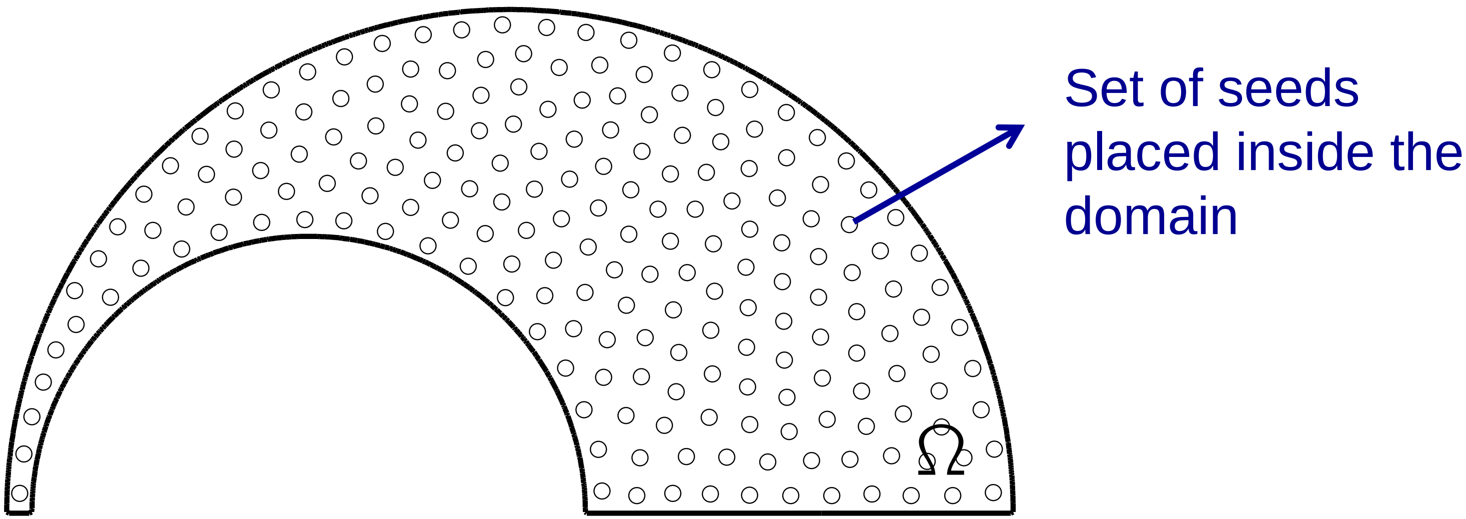

Talischi, C., Paulino, G. H., Pereira, A., & Menezes, I. F. M. *JSMO* 45(3), 309–328, 2012.

Instead of structured meshes, we use polygonal discretizations obtained from a Voronoi diagram

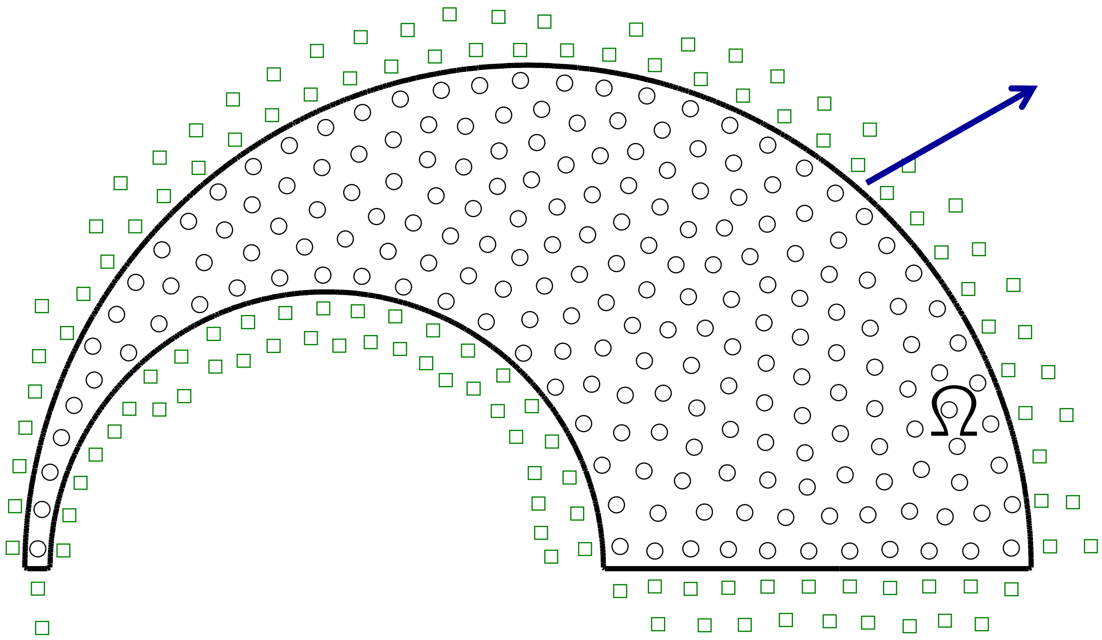

Reflections of seeds about the boundary

Talischi, C., Paulino, G. H., Pereira, A., & Menezes, I. F. M. *JSMO* 45(3), 309–328, 2012.

Instead of structured meshes, we use polygonal discretizations obtained from a Voronoi diagram

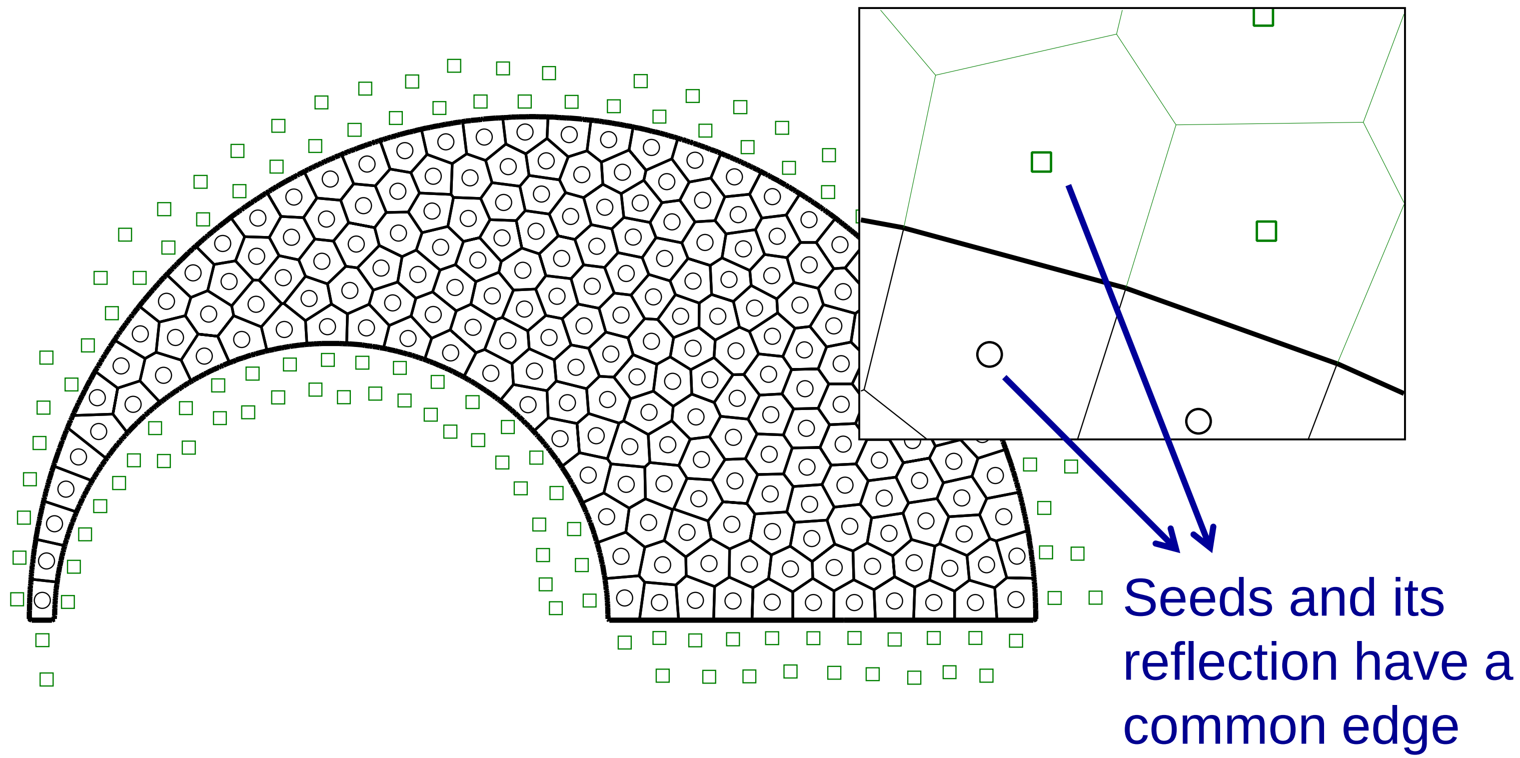

The mesh consists of the Voronoi cells associated with P:

$$\mathcal{M}_\Omega(\mathbf{P}) := \{V_y \in \mathcal{T}(\mathbf{P} \cup R_\Omega(\mathbf{P}); \mathbb{R}^d) : \mathbf{y} \in \mathbf{P}\}$$

Talischi, C., Paulino, G. H., Pereira, A., & Menezes, I. F. M. *JSMO* 45(3), 309–328, 2012.

Comparison of performance 10 sample random and CVT meshes with regular quadrilateral partition

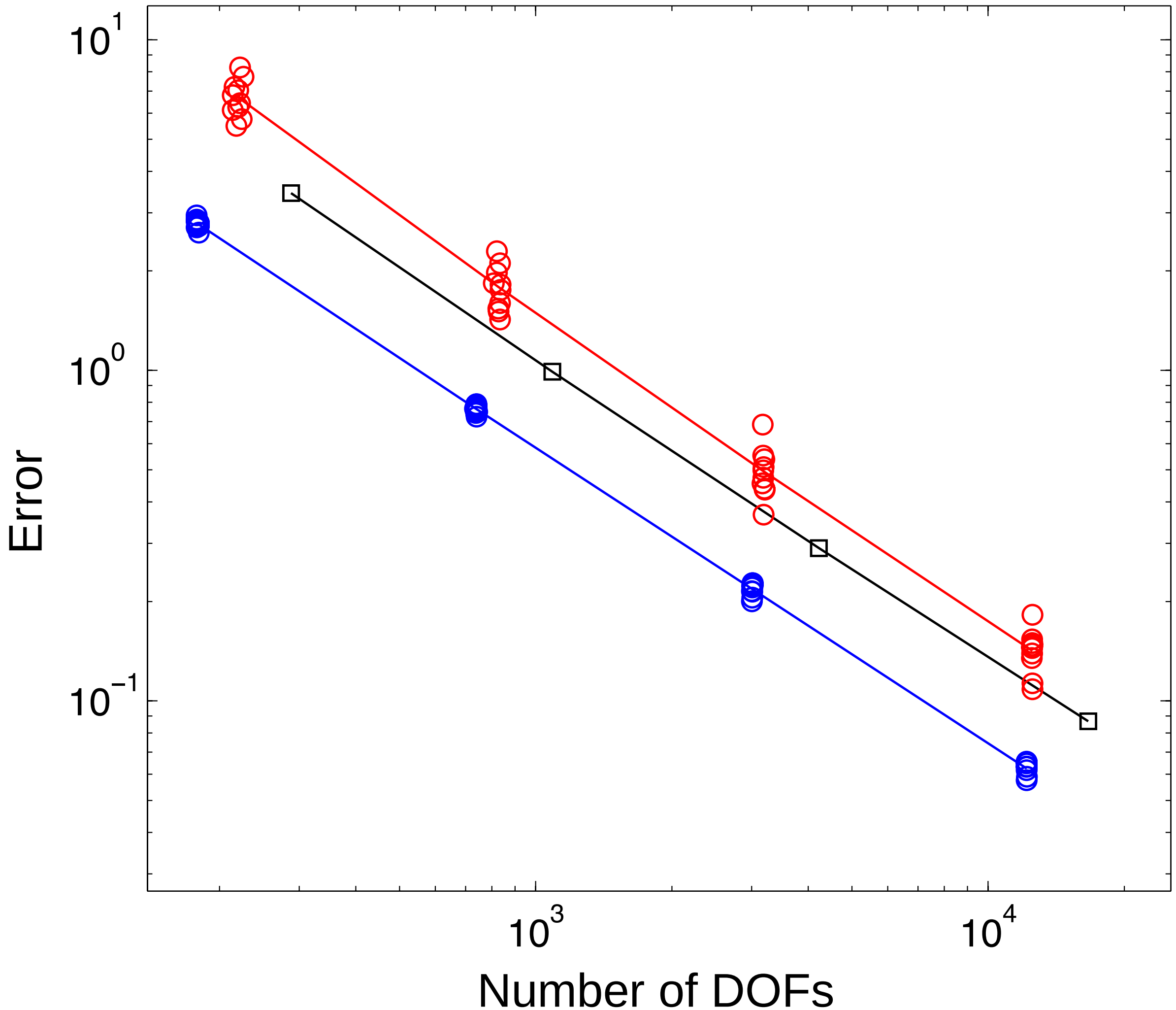

Random mesh

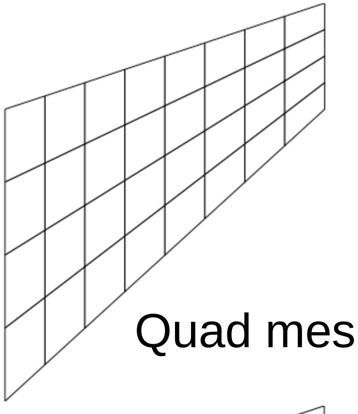

Quad mesh

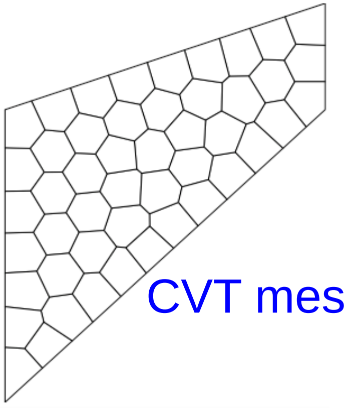

CVT mesh

[Talischi, Paulino, Pereira, Menezes, 2010]

Roughly 2x DOFs are needed with the quad mesh for the same level of accuracy

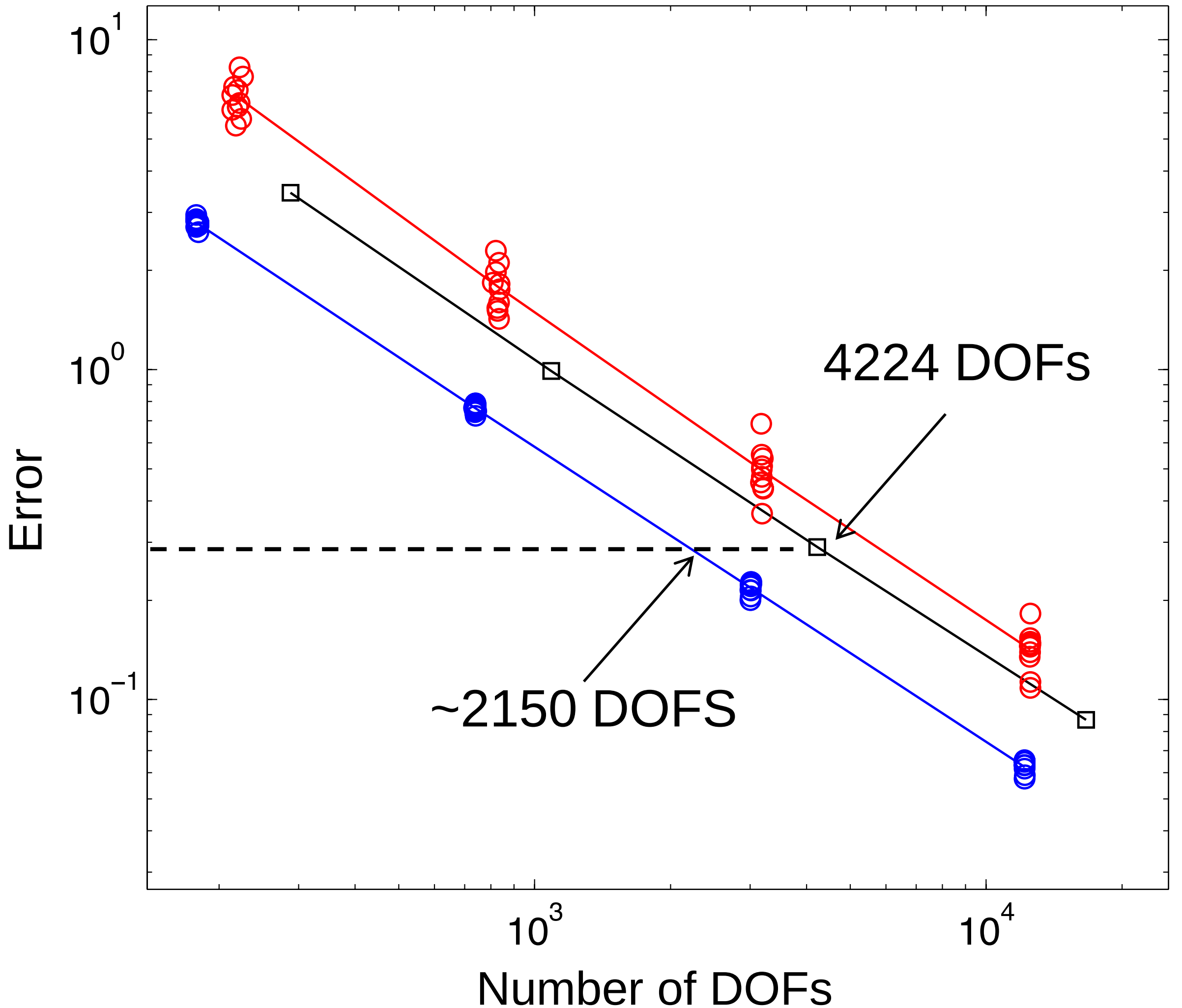

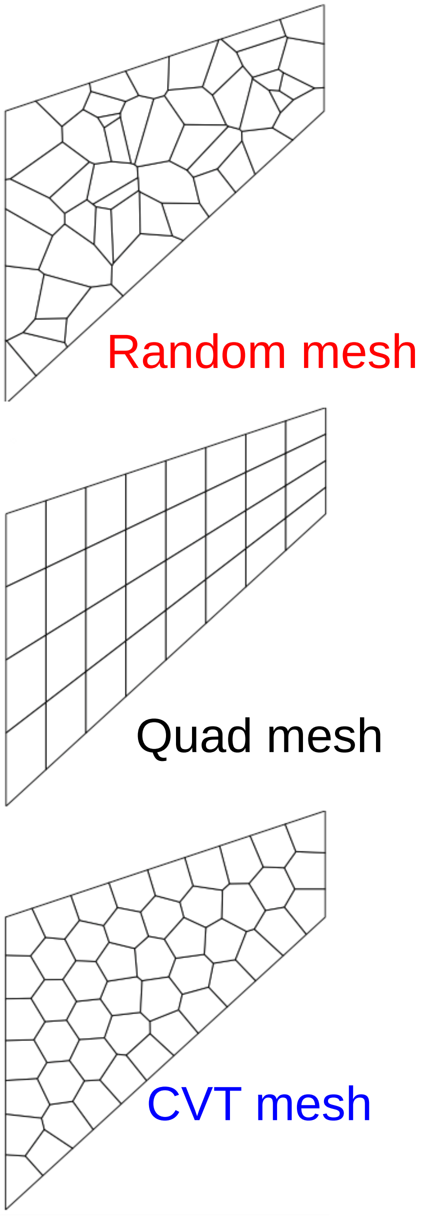

[Talischi, Paulino, Pereira, Menezes, 2010]

The factor is x1.6 for the triangulation (connecting centroid to the vertices) of CVT meshes

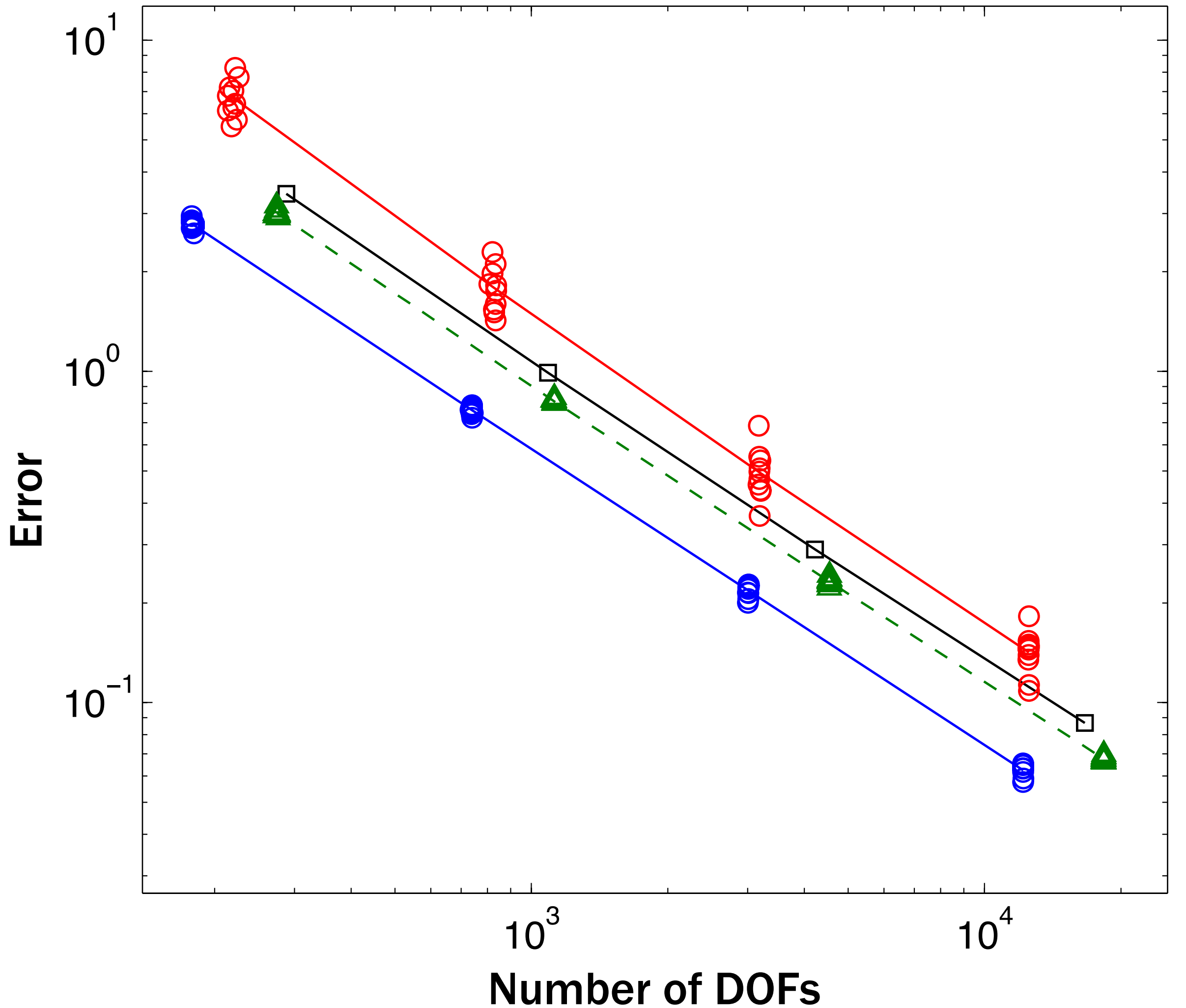

n triangles and one additional node for each *n*-gon

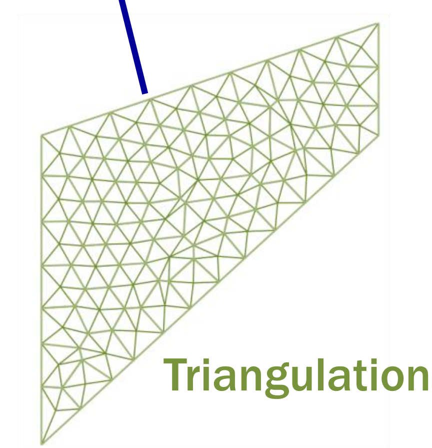

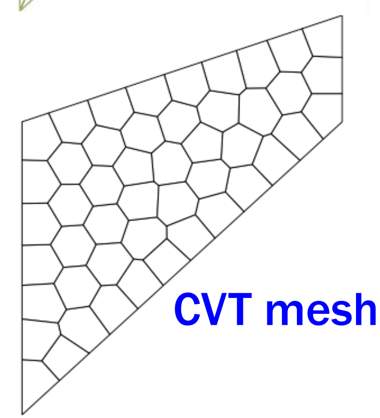

[Talischi, Paulino, Pereira, Menezes, 2010]

Instead of structured meshes, we use CVT polygonal discretizations

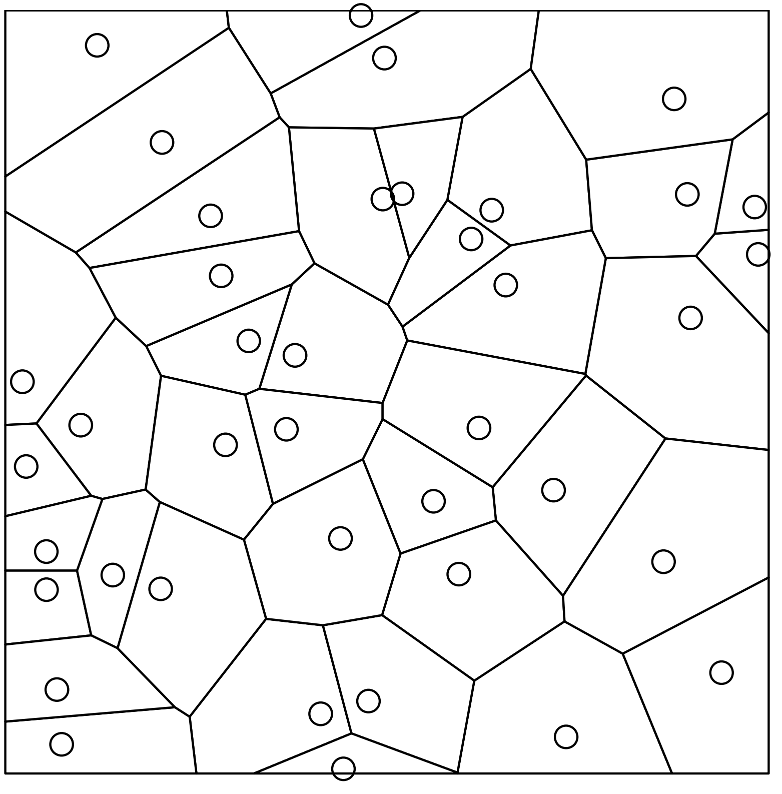

Generate a random point set inside the domain and construct the Voronoi diagram of each set

Talischi, C., Paulino, G. H., Pereira, A., & Menezes, I. F. M. *JSMO* 45(3), 309–328, 2012.

Instead of structured meshes, we use CVT polygonal discretizations

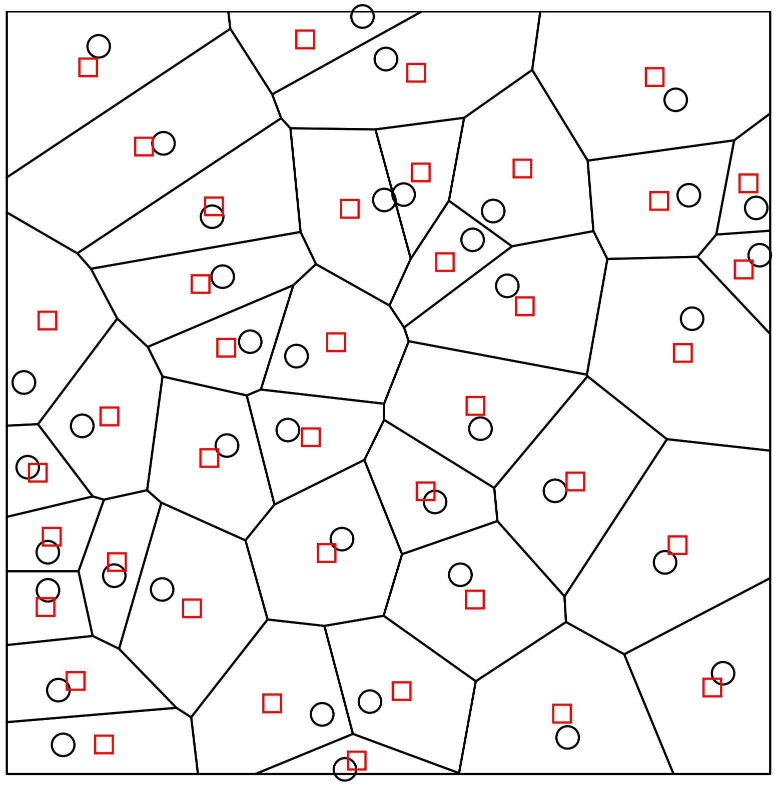

Each iteration consists of replacing each seed by the centroid of its cell

$$\mathbf{P}_{i+1} = \mathbf{L}(\mathbf{P}_i)$$

Lloyd's map

$$\mathbf{L}_y(\mathbf{P}) = \frac{\int_{V_y(P)\cap\Omega} \mathbf{x}\mu(\mathbf{x})\,d\mathbf{x}}{\int_{V_y(P)\cap\Omega} \mu(\mathbf{x})\,d\mathbf{x}}$$

Prescribed density function

Talischi, C., Paulino, G. H., Pereira, A., & Menezes, I. F. M. *JSMO* 45(3), 309–328, 2012.

Instead of structured meshes, we use CVT polygonal discretizations

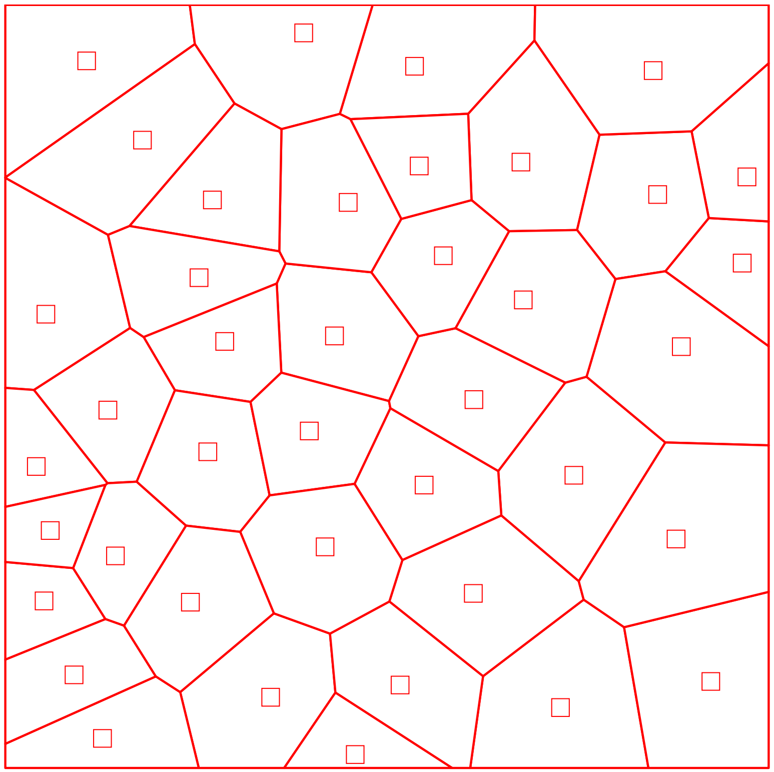

Each iteration consists of replacing each seed by the centroid of its cell

$$\mathbf{P}_{i+1} = \mathbf{L}\left(\mathbf{P}_i\right)$$

Lloyd's map

$$\mathbf{L}_y\left(\mathbf{P}\right) = \frac{\int_{V_y(P)\cap\Omega} \mathbf{x}\mu\left(\mathbf{x}\right) d\mathbf{x}}{\int_{V_y(P)\cap\Omega} \mu\left(\mathbf{x}\right) d\mathbf{x}}$$

Prescribed density function

Talischi, C., Paulino, G. H., Pereira, A., & Menezes, I. F. M. *JSMO* 45(3), 309–328, 2012.

Instead of structured meshes, we use CVT polygonal discretizations

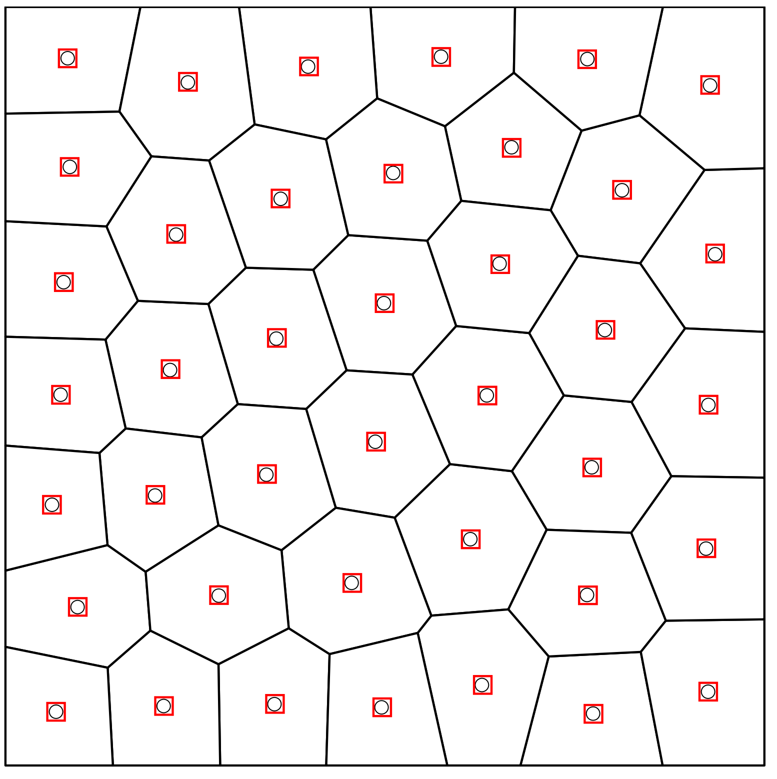

Each iteration consists of replacing each seed by the centroid of its cell

$$\mathbf{P}_{i+1} = \mathbf{L}\left(\mathbf{P}_i\right)$$

Lloyd's algorithm produces a Centroidal Voronoi Tessellation (CVT)

$$\mathbf{y} = \frac{\int_{V_y(P)\cap\Omega} \mathbf{x}\mu\left(\mathbf{x}\right) d\mathbf{x}}{\int_{V_y(P)\cap\Omega} \mu\left(\mathbf{x}\right) d\mathbf{x}}, \; \forall\, \mathbf{y} \in \mathbf{P}$$

Talischi, C., Paulino, G. H., Pereira, A., & Menezes, I. F. M. *JSMO* 45(3), 309–328, 2012.

We can construct graded meshes using a non-constant density function

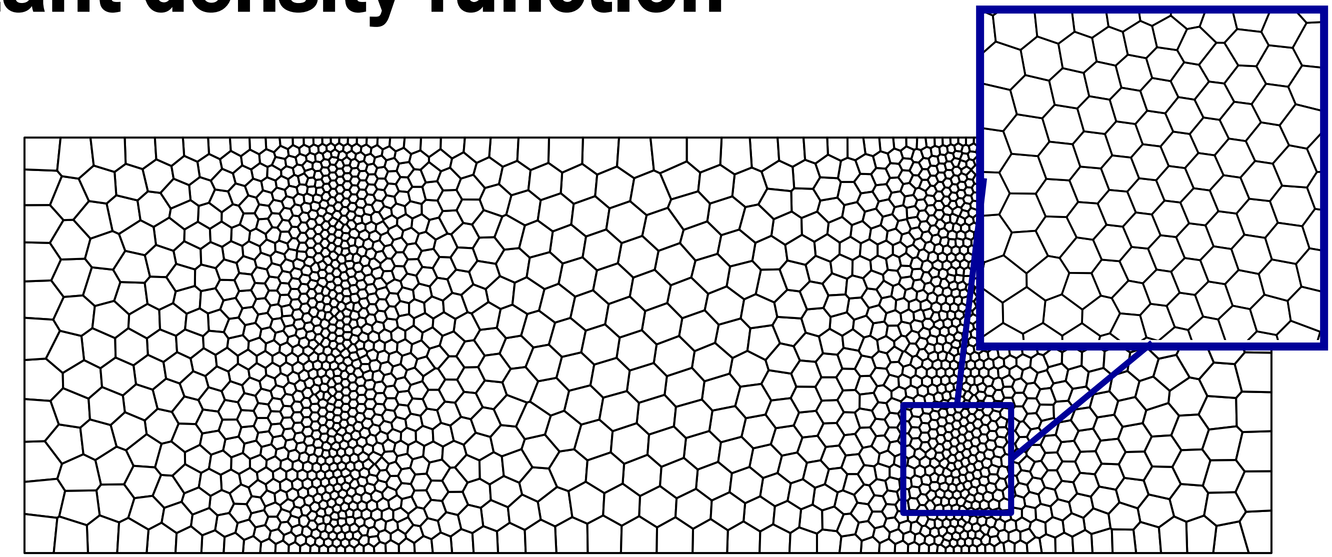

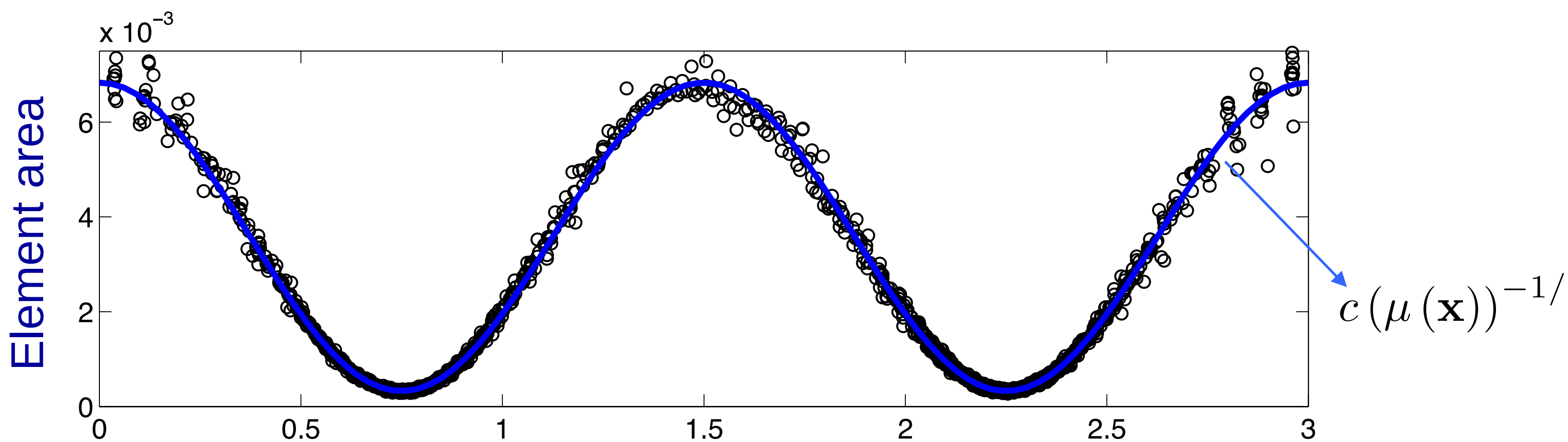

Talischi, C., Paulino, G. H., Pereira, A., & Menezes, I. F. M. *JSMO* 45(3), 309–328, 2012.